IEEE Access
Multidisciplinary ⋮ Rapid Review ⋮ Open Access Journal

Received 23 March 2024, accepted 6 April 2024, date of publication 11 April 2024, date of current version 18 April 2024.

Digital Object Identifier 10.1109/ACCESS.2024.3387664

RESEARCH ARTICLE

Multiobjective Model Predictive Control Based on Urban and Emission Macroscopic Fundamental Diagrams

ALESSIO TESONE[1,2], TAMÁS TETTAMANTI[3,4], BALÁZS VARGA[4], GENNARO NICOLA BIFULCO[1,2], AND LUIGI PARIOTA[1,2]

[1]Department of Civil, Architectural and Environmental Engineering, University of Naples Federico II, 80125 Naples, Italy
[2]Laboratory for Advanced Experiments on Roads and Traffic Environments—Centre for Advanced Technology and Metrology Services, University of Naples Federico II, 80125 Naples, Italy
[3]Systems and Control Laboratory, HUN-REN Institute for Computer Science and Control, 1111 Budapest, Hungary
[4]Department of Control for Transportation and Vehicle Systems, Faculty of Transportation Engineering and Vehicle Engineering, Budapest University of Technology and Economics, 1111 Budapest, Hungary

Corresponding author: Alessio Tesone (alessio.tesone@unina.it)

This work was supported in part by the Project Prin 2020 DigiT-CCAM—Digital Twins per la Mobilitã Cooperativa, Connessa e Automatizzata funded by the Italian Ministry of the University and the Research under Project 2020Z9HEMJ; and in part by the Ministry of Culture and Innovation of Hungary from the National Research, Development and Innovation Fund, through the TKP2021-NVA Funding Scheme, under Project TKP2021-NVA-02.

ABSTRACT Increasing motorization represents a severe problem worldwide, also affecting the emission levels of the road network. Accordingly, congestion management has obtained growing importance because of its strong economic, social, and environmental implications. Macroscopic Fundamental Diagram (MFD) based traffic control is a popular and efficient approach in this scientific field. In our research work the urban network has been divided into homogeneous regions, each of them characterized by its own MFD, and they are regulated using a network-level control scheme. The proposed Multiobjective Model Predictive Control (M-MPC) takes into account the congestion and CO_2 emission levels of the urban network, modelled by the emerging Emission Macroscopic Fundamental Diagram (e-MFD). The applied strategy has been demonstrated in a realistic traffic scenario (Luxembourg City) using validated microscopic traffic simulation. According to the introduced multiobjective approach, the control method can better exploit the road network capacity while efficiently reducing traffic-induced emissions.

INDEX TERMS Traffic congestion, emission, traffic management, MFD, e-MFD, multiobjective model predictive control, route guidance.

LIST OF NOTATIONS

α_{ij}	Accumulation rate.
Δ_i	Zone i oversaturation duration.
γ_i	e-MFD of region i.
λ	Cost function weigth.
$\mathcal{N}$	Set of urban regions.
$\mathcal{N}_c$	Set of regions of the city centre.
$\mathcal{N}_i$	Set of regions adjacent to i.
θ_{ij}^h	Route choices reflecting crossing zone h, starting from zone i, to reach zone j.
C_{ih}	Receiving capacity of region h from region i.
CS	Congestion severity.
E_{CO_2}	CO_2 normalized value of the city centre.
f_{ih}	Linear transfer flow.
FT_{MPC}	MPC feedback time.
G_i	Outflow of region i.
J_{1M}	CO_2 maximum value of the city centre.
J_{2M}	Production maximum value of the city centre.
k	Time instant.
K_p	Observation time.
k_p	Control time step.

The associate editor coordinating the review of this manuscript and approving it for publication was Ton Duc Do.

L_i	Average trip length of region i.
l_i	Length of road lane segment i.
M_{ij}^h	Transfer flow of vehicles that are in i and must cross to region h, in order to reach destination j.
M_{ii}	Internal trip completion rate of region i.
n_i	Total accumulation of region i.
N_p	Prediction horizon.
$n_{cr,i}$	Zone i critical accumulation value.
$n_{i,max}$	Maximum accumulation of region i.
n_{ij}	Number of vehicles in region i which have as their destination the region j.
$n_{peak,i}$	Zone i peak accumulation value.
P	Production normalized value of the city centre.
P_i	Travel production of region i.
$q_{\mathcal{I}}^w$	Zone $\mathcal{I}$ weighted average flow.
q_i	Measure flow on road lane segment i.
q_{ij}	Demand for vehicles, which are in region i to reach destination j.
s_P	Deviation between P and thd.
s_{CO_2}	Deviation between E_{CO_2} and thd.
$s_{i\%}$	Zone i oversaturation degree.
t_1	Time instant in which zone congestion appears on the first time.
t_2	Time instant in which zone congestion definitively ends.
T_p	Controller sample time.
thd	Threshold parameter.
co_{2i}	Measure CO_2 on road lane segment i.

I. INTRODUCTION

Traffic congestion is a growing problem and is responsible for many externalities, such as emissions and delays, and its management is vital in order to efficiently use the road infrastructure. Severe problems of urban traffic congestion have characterized many cities worldwide since most of the population activities are placed in the urban context. Indeed, since the 70s, different control strategies have been developed. In this regard, model-based control strategies are used in order to optimize urban network performance through the use of mathematical traffic models [1]. The most developed model-based control techniques are UTOPIA [2], MITROP [3], OPAC [4], PRODYN [5], RHODES [6], CRONOS [7] and MOTION [8]. These strategies use simple mathematical models offering limited prediction capabilities. Alternatively, some control techniques use very detailed micro and mesoscopic models that deal with local information of the network; it is worth mentioning in this regard, SCATS [9] and SCOOT [10]. Most parts of the above-mentioned control techniques applied on urban networks only focus on one part of the network, allowing local optimization [11]. In some cases, a local optimization could compromise the mobility performances of the rest of the uncontrolled urban network. Indeed, it is not easy to coordinate local controllers placed in different areas of an urban network, and then it is often not possible to guarantee the management of a large-scale network [12], [13], [14].

Another critical aspect is related to the computational burden associated with these approaches, in particular when they are based on very detailed traffic models since it is difficult to acquire and analyze in real-time, thereby imposing a computational burden on the system [15], [16]. An opportunity to solve this issue is represented by macroscopic traffic flow models such as Cell-Trasmission-model (CTM) and Link-Trasmission-model (LTM) that could be employed in control applications based on more aggregated information about the network [17]. This leads to increasing interest in research about the topic of network-level traffic control characterized by low computation effort [18]. In this regard, control techniques based on the paradigm of the Macroscopic Fundamental Diagram (MFD) [19] gained great interest [20].

A. LITERATURE REVIEW OF MFD BASED CONTROL APPROACHES

The MFD provides aggregated information through the use of a concave relationship between only two variables, the accumulation (e.g. link-length weighted average density/number of vehicles), and the production (e.g. link-length weighted average flow) which can be measured in real-time, and thus strongly reduces the computational burden of the measurement procedure inside a control framework [21], [22].

For the above reason, the MFD modelling paradigm tool has gained a lot of popularity in managing network-level control techniques such as Perimeter control and Route Guidance. Typically the MFD is defined for different portions of an urban network, generating the so-called multireservoir models that allow the performing of Hierarchical control schemes [13], [23], [24]. In this hierarchical scheme, at the upper level, the controller uses the MFD information to understand the congestion level of each region and consequently manipulates the macroscopic traffic flows through an inter-regional actuation system. At the lower level, some local controllers are used to regulate the mesoscopic traffic flows through an intraregional actuation system (e.g. signalized intersections, variable message signs).

A lot of works in literature combine the modelling paradigm of the MFD with the use of the Model Predictive Control (MPC) technique [25]. The motivation for the aggregation of the MFD paradigm inside the MPC framework is the computational complexity of the MPC, scaling poorly for high-dimensional and non-convex problems [26]. One of the first works using this control paradigm is proposed by [27], where the authors solved an optimal perimeter control problem, also known as gating, by using the MPC, where the prediction model and the plant are formulated by MFD. The gating protects a specific network area by limiting access to it using a traffic light system. But this strategy increases the waiting time and the queue could

compromise the congestion levels of the other zones. The Perimeter Control problem has become the main object concerning network-level control and different aspects of the problem have been deeply investigated [28], [29], [30], [31], [32]. Indeed, the Perimeter control problem is still nowadays capturing the attention of researchers [33], [34], [35], [36].

An alternative to Perimeter Control is the Routing strategy, also known as Route Guidance, used to suggest alternative paths offered by the road infrastructure. This application has some advantages since its applicability suits well in a period in which the spread of information is guaranteed by the development of different technological systems such as smartphones providing floating car data (FCD) [37], [38], and emerging vehicle-to-everything (V2X) communication technologies [39], [40], [41]. A second advantage relies on the minor infrastructure costs since it is not necessary to control the traffic light system, but the usage of Intelligent Transportation Systems (ITS) technologies such as Variable Message Signs (VMS) panels and emerging communication technologies represents a valid way to spread the control decisions among the network users [42], [43]. One of the most relevant application in this field was proposed by [44], where the authors used the MFD and MPC-based approach to deal with traffic congestion mitigation. Most recently, in [13] the authors show the great potential of a large-scale Route Guidance scheme in achieving coordination and efficient use of network capacity, leading to increased mobility. Additionally, in [45] the authors demonstrated how the integration of a Route Guidance system in a Perimeter Control scheme improves the performance of the MPC and MFD-based controller.

B. LIMITATIONS AND CHALLENGES

Although very significant and promising, all the previous applications were characterized by a common aspect related to experimental validation in a simplified context. In all the depicted cases, indeed, the highlighted strategies have been applied in toy networks whose topology was not related to existing road infrastructures. Furthermore, no MFD curves calibration activity was carried out, and pre-defined curve parameters established in the work of Yokohama [19] were used for them. In this regard, typically, a unique reference MFD curve was used for all the network regions [13], [14], [27], [28], [29], [30], [31], [45], and [46]. It has been extensively demonstrated that traffic congestion is typically heterogeneously distributed along the network [24], [47], [48], [49], [50]. In this regard, the partition procedure is carried out in order to guarantee homogeneous regions in an urban network. As a consequence, it is quite improbable that the different regions obtained by the partition procedure have the same topology. Consistently with results of [51], specific curves should be defined for zones with different topological characteristics.

Another relevant aspect concerns the proper representation of the response of the controlled system and/or of the mechanisms underlying the actuation system. These assumptions could compromise the prevision procedure carried out by the MFD-model dynamics in the MPC framework. Undeniably, a simplified and straightforward response of the traffic context to the control actuation could be not enough to test and evaluate the system's robustness in real-world applications. The approaches introduced by [13], [27], [28], [29], [30], [31], and [45], are characterised by this limitation. Simulating the controlled environment by means of an external tool could help to overcome the issue ([52], [53], [54]). Specifically, a microscopic traffic simulator could strongly improve the realism of the application case study, given its ability to emulate more precisely the stochasticity of flow propagation and traffic dynamics. In this regard, during the last years some efforts have been made in order to provide more realistic case studies through the usage of Simulation tools in [55], [56], and [57]. Moreover, typically the operating scenarios of these works are not based on real (historical data) data taken from the field, and the provided network infrastructures do not cover the dynamics of a whole city. In this regard, in [55] the demand generated with the traffic simulator Aimsun[1] does not cover a whole day. In addition, the scenario created does not cover the whole city of Barcelona, but $12 km^2$ of it (600 intersections and 1500 links have been modelled in the network). In [56] the test network is made up of the $3rd$ and $6th$ districts of Lyon and the city of Villeurbanne (3363 links) while in [57] the test site is a 64.7 km^2 area of Downtown San Francisco. The ability of the proposed approaches to improve the mobility performances of the tested areas has been demonstrated, but a question remains about what happens in the rest (uncontrolled) portion of the network. Certainly, all the applications mentioned focus on analyzing and explaining their outcomes by referencing the section of the network where control is implemented. However, there is a notable absence of modelling the entire network to assess the controller's impact beyond the specific test case.

A shared characteristic among all the examined works is the common objective of control: either to minimize the overall network travel time or maximize the network throughput (i.e. the maximum rate of movement or flow of vehicles through a transportation network) [36]. Nevertheless, it is widely acknowledged that transportation systems exhibit conflicting dynamics, such as the tension between maximizing network throughput and minimizing network emission levels. For instance, the pursuit of higher network throughput could potentially result in elevated emission levels, as a larger volume of vehicles moves through the infrastructure. Hence, there is an intriguing prospect to develop a control framework that can effectively balance these different aspects simultaneously. The need to develop a monitoring system of network-wide emissions is recently gaining popularity [58], [59]. The works of [60] and [61] open the door for research in this direction. In particular, in [60] the authors found a relationship between the network

[1] https://www.aimsun.com/aimsun-live

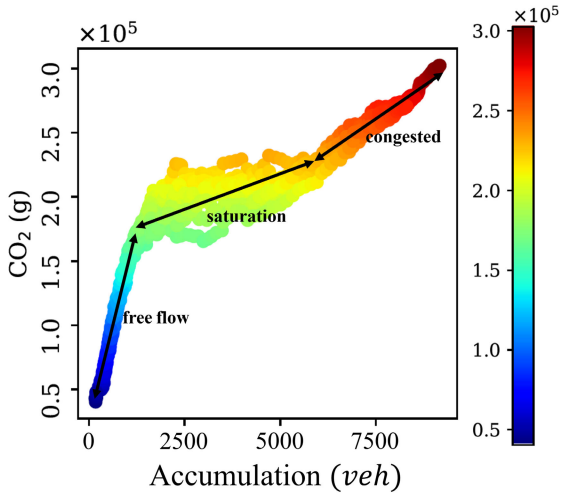

FIGURE 1. An empirical e-MFD curve, [62].

aggregated variable average speed and the emission levels of the network. In this way, they introduced new aggregated curves called emission-Macroscopic Fundamental Diagrams (e-MFDs). So, the e-MFD relates aggregate traffic dynamics to emissions providing a mechanism to apply network-wide traffic control and demand management policies to emissions reduction objectives. This is confirmed in [62] in which the authors explored the three branches of the e-MFD (i.e. free flow, saturation and congested). In this regard, in Fig. 1 the empirical e-MFD points collected by [62] are reported by highlighting the free flow, the saturation and the congested branches of the curve. The challenge of striking a balance between congestion alleviation and emission reduction is notably intricate, particularly when the network operates at level of accumulations up to the saturation regime. Many network control strategies focus on steering the network into the saturation domain, where throughput is maximised. However, by analysing the e-MFD curve, it becomes evident that emission levels increase proportionally to the accumulation values. Therefore, while a traffic management policy maximizes throughput, it may cause excessive emission levels. Moreover, the importance of adopting a harmonized approach in urban management strategies, which reconciles divergent objectives through the employment of multi-objective methodologies, is underscored by recent literature works [63], [64].

C. CONTRIBUTIONS

The objective of the current research is to make a further step in the investigation of the MPC and MFD-based network control. Indeed, the proposed application falls in the stream of hierarchical network-level control where the upper level optimizes network performance based on route choice recommendations through different regions, whereas the lower-level control performs a path assignment mechanism satisfying the regional split ratios established by the MPC controller at the upper level, and is inspired by the modelling representation introduced in [12], [13], and [27]. However, the advocated improvement with respect to the literature concerns several different aspects that make this contribution interesting.

First of all, the strategy is validated here on a large-scale scenario, representing the whole city of Luxembourg; this represents a unique case in the analyzed literature. The complexity of the current application not only concerns the width of the scenario itself, but also the realism of the controlled system responses, since the Luxembourg City demand and supply system is reproduced in the microscopic traffic simulator SUMO [65], and is based on the mobility studies performed in [66] that deal with city traffic characteristics over recent years available on LuxTram official Internet site.[2] The higher realism has also led to an increased need for calibration activities which confirmed that different zones with different characteristics exhibit different dynamics (and then MFD curves).

A second element of interest in the paper concerns the investigation of the effects of the control when different conflicting objectives are considered. In particular, the CO_2 aggregated emission levels of the urban network, modelled by the emerging e-MFD, are taken into account in the controller objective function in different combinations with the generally used throughput maximization objective. Notably, e-MFD curves have been calibrated specifically for each zone. Finally, to implement the M-MPC a weighted cost function in the MPC framework has been introduced, and the original modelling framework has been improved with a real-time mechanism for setting the value of the weights according to the current network condition in order to balance throughput maximization and CO_2 levels minimization. The multiobjective strategy has been benchmarked with respect to simpler strategies, specifically:

- A Dijkstra Routing algorithm based on instantaneous cost and user optimum already implemented in SUMO;
- A mono objective MPC framework for the maximization of the network throughput;
- A mono objective MPC framework for the minimization of the emission levels.

II. METHODS

An MPC-based control strategy is implemented in this work to solve a routing problem. The MPC framework is integrated into a simulation environment, and it is tested and validated in a realistic traffic scenario. In Fig. 2 the block diagram of the control scheme is reported. The plant is the urban network, i.e. the physical system whose behaviour should be optimized. The network is divided into N regions, each of which is characterized by its own MFD curve used to estimate its congestion level; this is aggregated information based on the accumulation values of each zone (the number of vehicles in the region) through the MFD modelling paradigm. The state variable $x(k)$ (veh) is an array of N elements containing

[2]https://www.luxtram.lu

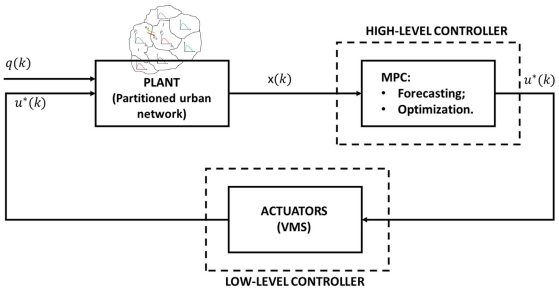

FIGURE 2. The control loop scheme.

the accumulation level of each zone of the network at the time instant k. The state variable at the time instant k initializes the forecasting model that is used in the MPC framework in order to solve in real-time the optimization problem. The optimal value of the control variable $u^*(k)$ represents the optimal flow split ratios among the regions (i.e. regional route choices) at the time instant k that the users of the network should follow in order to improve the network performances. This optimal sequence is applied, through a proper actuation system, to the whole network, by closing the loop. The control variable $u^*(k)$ and the traffic demand $q(k)$ (veh/sec) at the time instant k alter the network behaviour according to the loop principle proposed in Fig. 2. However, the MPC represents the high-level controller and the optimal value of the control variable is the input of a lower-level controller. The spread of the control signal throughout the urban network is applied aiming to enhance the realism and applicability of this routing strategy. This is achieved by replicating the functionality of a conventional Intelligent Transportation System (ITS) technology, specifically Variable Message Signs (VMSs).

Of course, VMSs are located in specific points of the network, here defined SWitching Points (SWPs), that are used to spread routing information in order to actuate the optimal route choices. On the SWPs, the vehicle receives the rerouting suggestion and it can change its route.

In the MPC framework, during the whole observation time K_p $[sec]$, the controller every control time step $k_p = nT_p$, $n \in \mathbb{N}$, solves a constrained optimization problem by using a forecasting model that predicts, within a prediction horizon window N_p, the state variable values of the plant whose behaviour it wants to optimize [25]. The parameter T_p $[sec]$ represents the controller sample time that establishes its operating frequency, while the prediction horizon window N_p is an integer number expressed as the number of control time steps k_p in which the forecasting procedure is carried out.

A. THE MFD AND E-MFD MODELLING TOOLS

In this approach, we use the MFD to have an aggregated representation of the traffic flow dynamics of the urban network. The MFD provides a relationship between accumulation (the number of vehicles in the district) and production (the weighted average flow in the district). Fig. 3 shows a typical MFD curve of an urban network region distinguishing each operating condition on it (free flow,

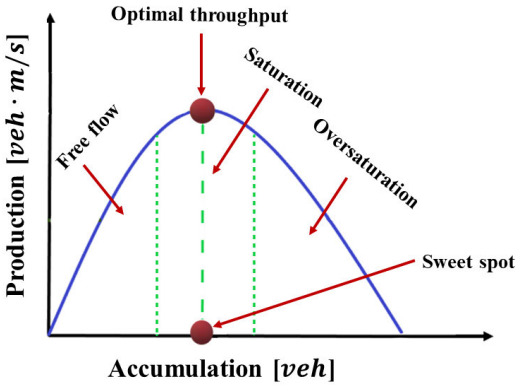

FIGURE 3. A region MFD curve.

saturation, oversaturation). In the free flow regime, the accumulation values are lower than the critical accumulation value (i.e. sweet spot), and to an increase of accumulation, an increase of production corresponds. Beyond the critical value, the production decreases with the accumulation increasing since the region's capacity is reached. In the saturation regime, the region achieves its optimal operating conditions since the production is maximized and the zone reaches the optimal throughput. We want to solve a routing strategy in order to drive the network as nearest possible to this operating domain, by controlling the accumulation values near the critical one through an adequate manipulation of the regional route choices. To apply the proposed control strategy, the urban network is divided into different regions, each of which is characterized by its MFD, as represented in Fig. 4. Furthermore, an e-MFD curve has been associated with each zone. In this work, the region e-MFD provides a relationship between the zone accumulation and the CO_2 level expressed in kg, but this approach could be extended for other exhaust emissions such as NO_x and PM_x. Nevertheless, focusing only on optimizing for CO_2 is adequate, given that the e-MFD curves for various pollutants exhibit strong correlations. Again, there is a need for proper calibration of each curve, since [60], through experimental analysis, suppose that the e-MFD might depend (similarly to the MFD) on the spatial distribution of congestion, the driver adaptability, and the unloading demand profile [24], [48]. In this regard, there is some similarity between aspects that affect the shape of an MFD (link length, signal settings, signal offsets, spatial distribution of congestion) and the shape of an e-MFD curve. Furthermore, emissions are significantly influenced by local congestion phenomena such as stop-and-go traffic, that are correlated with aggregated traffic quantities. Specifically, the highest emission rates are linked to vehicle accelerations, and the duration spent in acceleration is connected to the frequency of stops each vehicle encounters during its path. For these reasons, we assume that the same zone partitioning of the network is used for the calibration of MFD and e-MFD curves. It is worth noting that in [67] some properties of the e-MFD have been highlighted. In this regard, it has been demonstrated that the macro-emission reaches its peak value

at the peak traffic flow (i.e. the MFD sweet spot point). The observations in [67] showed that the flow breakpoint around the sweet spot point segregates the e-MFD diagram into three phases: stable (i.e. free flow), saturation and unstable (i.e. congested). Indeed, the emission rate increases rapidly with an increase in density/accumulation and reaches a saturation level of maximum at the sweet spot value during the loading phase. Then, the flow breakdown occurs and the emission rate ($[ton/hour]$) starts to decrease by accumulation increase until the recovery (unloading phase) begins. It should be noted that, beyond the sweet spot point, during the unstable phase, vehicles spend more time on the network and produce more emissions. Therefore, although the emission rate decreases during the unstable phase, vehicles spend more time in the network and generate more emissions. Indeed, more congestion results in more cumulative emissions overall. This is confirmed in [62] in which the authors explored the three branches of the e-MFD already highlighted in Fig. 1. In accordance with the proposal outlined in [62], the development of the emission monitoring system is delineated into distinct phases. Initially, the acquisition of network emission and traffic data is undertaken, with a specific emphasis on utilizing microscopic simulation software to emulate real-world conditions. This process involves incrementally augmenting traffic demand flow until the network attains gridlock, facilitating an examination of e-MFD dynamics across congested and free-flow regimes. Subsequently, in the second phase, the correlation between the collected traffic data and network emission levels is elucidated, enabling the calibration of e-MFD curves essential for monitoring emissions on a network-wide scale. To conclude, it is obvious that by relating aggregate traffic dynamics to emissions, the e-MFD could provide a mechanism to link network-wide traffic control and demand management policies to emissions reduction objectives. For this reason, in this research, we propose a multiobjective controller trying to find a good compromise between the maximization of the network throughput and the minimization of network emissions.

B. THE MACROSCOPIC TRAFFIC FLOW MODEL

The proposed control strategy needs a mathematical model to perform the forecasting procedure within the optimization problem. In this regard, the mathematical model in [12] is used to apply the forecasting procedure. For each region i a set of equations is provided to describe the evolution in time of the zone i accumulation.

$$n_{ii}(k+1) = n_{ii}(k) + T_p\Big(q_{ii}(k) - M_{ii}(k) - \sum_{h\in\mathcal{N}_i} {M^h}_{ii}(k) + \sum_{h\in\mathcal{N}_i} {M^i}_{hi}(k)\Big), \quad (1)$$

$$n_{ij}(k+1) = n_{ij}(k) + T_p\Big(q_{ij}(k) - \sum_{h\in\mathcal{N}_i} {M^h}_{ij}(k) + \sum_{h\in\mathcal{N}_i} {M^i}_{hj}(k)\Big), \quad (2)$$

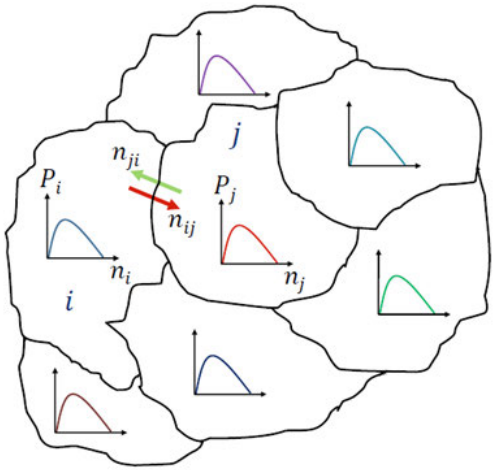

FIGURE 4. Network zoning [12].

while the total accumulation of zone i is computed as follows:

$$n_i(k) = \sum_{j\in\mathcal{N}} n_{ij}(k), \quad (3)$$

where:

- $\mathcal{N} = 1, 2, .., N$ represents the set of regions of the urban network;
- $\mathcal{N}_i$ indicates the set of all regions adjacent to region i;
- $q_{ij}(k)[veh/s]$ represents the demand for vehicles, which are in region i to reach destination j, aggregated in the sample time T_p, at time instant k;
- $n_{ij}(k)$ the number of vehicles in region i which have as their destination the region j at the time instant k;
- $M_{ii}(k)[veh/s]$ is the internal trip completion rate of region i (without going through another region);
- ${M^h}_{ij}(k)[veh/s]$ the flow of vehicles that are in i and must cross to region h, in order to reach destination j (transfer flows).

The total accumulation values of each zone compose the state variable x in the array form: $x = [n_1(k)\, n_2(k) \ldots n_N(k)]$. The transfer flow ${M^h}_{ij}$ represents the minimum between the sending flow from the region i to the adjacent region h and the receiving capacity of the receiving region h $C_{ih}(n_h(k))$. This flow capacity is presented as a piecewise function of the receiving zone accumulation n_h [12]. It is introduced to mitigate the occurrence of overflow events within specific areas; in other words, each region, denoted as i, possesses a maximum accumulation, $n_{i,max}$ such that:

$$0 \le n_i(k) \le n_{i,max}. \quad (4)$$

The transfer flows and the internal trip completion rates have the following expression:

$${M^h}_{ij}(k) = \min\Big(C_{ih}(n_h(k)), {\theta^h}_{ij}(k)\frac{n_{ij}(k)}{n_i(k)}\frac{P_i(n_i(k))}{L_i}\Big), \quad (5)$$

$$M_{ii}(k) = \theta_{ii}(k)\frac{n_{ii}(k)}{n_i(k)}\frac{P_i(n_i(k))}{L_i}, \quad (6)$$

in which:

- $P_i(n_i(k))$ represents travel production, calculated through the MFD function $[(vehm)/s]$;
- $\theta^h{}_{ij}(k) \in [0, 1]$ and $\theta_{ii}(k) \in [0, 1]$ the route choices, that reflect the percentage of choices of the route that involves crossing zone h, starting from zone i, to reach zone j and the percentage of choices of the route that involves remaining in zone i, to reach zone i, respectively;
- L_i, the average trip length $[m]$, independent of the time and the destination area associated with the crossing of zone i.

The values $\theta^h{}_{ij}(k)$ compose the control variable $u(k)$ in the form $u = [u^1\ u^2 \dots u^N]$, where:

$$u^h = \begin{bmatrix} \theta^h_{11} & \theta^h_{12} & . & . & . & \theta^h_{1N} \\ \theta^h_{21} & \theta^h_{22} & . & . & . & \theta^h_{2N} \\ . & . & . & . & . & . \\ . & . & . & . & . & . \\ . & . & . & . & . & . \\ \theta^h_{N1} & \theta^h_{N2} & . & . & . & \theta^h_{NN} \end{bmatrix}, \quad \forall h = 1, 2, \dots, N.$$

In Eq. (5) it is clear that there is a non-linear relationship between transfer flows and accumulation. A linearization is carried out in order to implement a linear optimization problem. Some dummy variables are used:

- The accumulation rates $\alpha_{ii}(k) = n_{ii}(k)/n_i(k)$ and $\alpha_{ij}(k) = n_{ij}(k)/n_i(k)$, $\forall i, j \in \mathcal{N}$, measured every time that we roll the horizon and considered constant during the optimization horizon;
- The new decision variables $f_{ii} = \theta_{ii}G_i(n_i(k))\alpha_{ii}$ and $f_{ih} = G_i(n_i(k))\sum_{j\in\mathcal{N}} \theta^h{}_{ij}(k)\alpha_{ij}(k)$, $\forall i, j \in \mathcal{N}, h \in \mathcal{N}_i$, where the function $G_i(n_i(k))$ represent the outflows of the regions of interest $P_i(n_i(k))/L_i$.

Similar to numerous other studies, the expression for the capacity $C_{ih}(n_h(k))$ in Equation (5) is excluded, as observed in [12]. This exclusion is justified from a control perspective, deeming it unnecessary. The implemented control actions are designed to prevent the system from operating in states approaching gridlock, making the modelling of receiving capacity unnecessary within the M-MPC problem. This assurance is further reinforced by incorporating the constraint (4) in the formalization of the optimization problem. Moreover, a simple assumption is considered: the source-destination information regarding the zone accumulations is not tracked, since is not necessary for control purposes. So the set of equations (1), (2) and (3) becomes:

$$n_i(k+1) = n_i(k) + T_p\Big(q_i(k) - f_{ii}(k) - \sum_{h\in\mathcal{N}_i} f_{ih}(k) + \sum_{h\in\mathcal{N}_i} f_{hi}(k)\Big). \quad (7)$$

C. HIGH-LEVEL CONTROLLER: MULTIOBJECTIVE MPC (M-MPC)

Eq. (7) is used to perform the forecasting procedure inside the optimization problem. The goal is to optimize the congestion and emission levels in the city centre, where the traffic situation is the most critical. In this regard, the objective function has the following expression:

$$J(k) = \lambda\frac{J_1(k)}{J_{1M}} - (1-\lambda)\frac{J_2(k)}{J_{2M}}, \quad (8)$$

where:

- $J_1(k) = \sum_{i\in\mathcal{N}} \gamma_i(n_i(k))$ represents the CO_2 level of the urban network of the city centre, estimated by using the e-MFD curves γ_i of each region i;
- $J_2(k) = \sum_{i\in\mathcal{N}} L_i(f_{ii}(k)+f_{ih}(k))$, $\forall h \in \mathcal{N}_i$ represents the Travel Production of the city center;
- $\lambda \in [0; 1]$ is the weight used to give priority to an aspect or the other one.

In Eq. (8) the two cost functions J_1 and J_2 are normalized by their maximum values J_{1M} and J_{2M} respectively, in order to make a consistent comparison between the two quantities. The parameters J_{1M} and J_{2M} were determined during the calibration processes, through to the collection of simulation data. Therefore, the optimization problem to be solved from an MPC perspective is as follows:

$$\min_{\theta^h{}_{ij}(k)} \sum_{k=k_p}^{N_p-1} J(k) \quad (9)$$

subject to (7), (4),

$$f_{ii} = \theta_{ii}G_i(n_i(k))\alpha_{ii}, \quad (10)$$

$$f_{ih} = G_i(n_i(k))\sum_{j\in\mathcal{N}} \theta^h{}_{ij}(k)\alpha_{ij}(k), \quad (11)$$

$$\sum_{h\in\mathcal{N}_i} \theta^h{}_{ij}(k) = 1, \quad (12)$$

$$0 \le \theta^h{}_{ij}(k) \le 1, \quad \forall i, j \in \mathcal{N}, h \in \mathcal{N}_i, h \ne i, \text{ with } k = k_p, k_p+1, \dots, k_p+N_p-1. \quad (13)$$

The objective function takes into account the congestion level of the city centre and the CO_2 levels at the same time by predicting the network congestion state in the following N_p control time steps. The decision variables are the route choices $\theta^h{}_{ij}$, the MPC computes in real-time the optimal sequence of them in order to minimize the levels of congestion (i.e. maximize the travel production) and CO_2 in the city centre.

In this strategy, the value of the weight λ in the cost function (8) is set in real-time (i.e. each control time step), according to a specific weight-assignment criterion. Once the value of λ has been established by the assignment criterion, the cost function (8) is set accordingly and the MPC can start the optimization procedure. The assignment criterion is based on the comparison between the current normalized values of the city centre emission and production at time instant k, called $E_{CO_2}(k)$ and $P(k)$, respectively. The goal is to set λ in order to assign the weight in (8) that guarantees an MPC optimization providing Emission levels at least lower than a given threshold of its maximum value (i.e. $thd \in [0, 1]$)

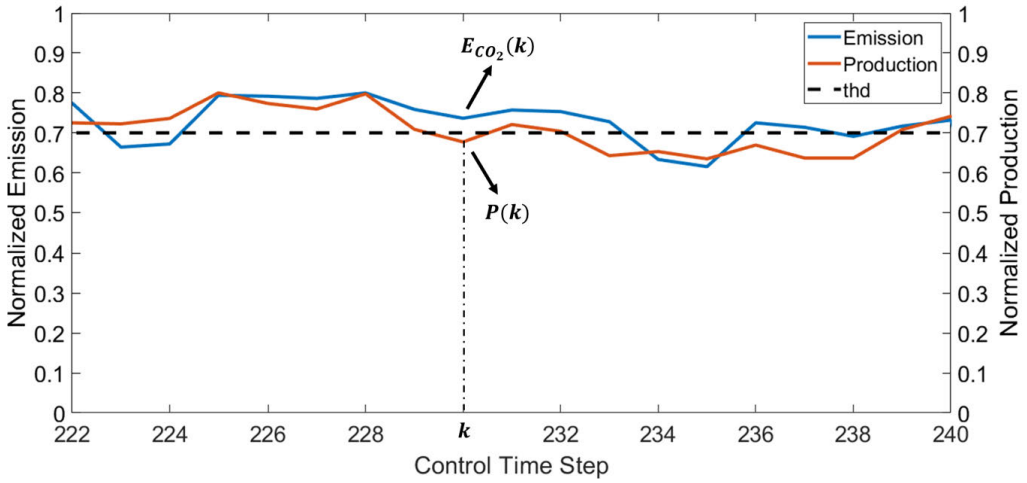

FIGURE 5. Time evolution of normalized emission and normalized production w.r.t. the chosen *thd* and comparison in the time step *k*.

and Production levels higher than *thd*. An example of the criterion application can be found in Fig. 5 which shows the comparison of $E_{CO_2}(k)$ and $P(k)$ with a value of *thd* fixed to 0.7. The comparison is made each time we roll the horizon and it can lead to 4 different cases covering all the possible combinations between the normalized values of CO_2, Production, and *thd*. In each case a specific value is assigned to λ and in this framework, the only parameter that needs to be calibrated is the threshold value *thd* since it is fixed a priori. The list of the 4 possible cases resulting from the comparison is reported below:

1 $E_{CO_2}(k) \leq thd$ and $P(k) \leq thd$;
2 $E_{CO_2}(k) \leq thd$ and $P(k) > thd$;
3 $E_{CO_2}(k) \geq thd$ and $P(k) > thd$;
4 $E_{CO_2}(k) \geq thd$ and $P(k) \leq thd$.

In the first case, according to the expression of the cost function (8), λ is set to 0 because the control needs to guarantee a level of city centre production of at least the *thd* value. In the 2nd case, there is no need to apply the control since city centre emission levels don't exceed the *thd* and production is higher than the threshold. The 3rd case is the opposite of the 1st one, so λ is set to 1. Finally, in the 4th case, the controller needs to act in both directions (minimization of E_{CO_2} and maximization of P); it is needed to take into account the deviations between E_{CO_2} and *thd* that is called $s_{CO_2} = \left|E_{CO_2} - thd\right|$ and between P and *thd*, called $s_P = |P - thd|$. The 4th case includes three different subcases:

a. $s_p > s_{CO_2}$, in which λ is set to s_{CO_2};
b. $s_p < s_{CO_2}$, in which λ is set to $thd + s_{CO_2}$;
c. $s_p = s_{CO_2}$ in which λ is set equal to $1/2$.

All the rules mentioned above are defined a priori and they include all the possible states that the network could assume. It's noteworthy that the specified criterion enhances the flexibility of the cost function by establishing a direct correlation between the weight values in the cost function (8) and the network states related to congestion and emission. An alternative approach could involve integrating constraints such as emission thresholds or throughput, either as hard constraints or as soft constraints using barrier functions. However, adopting such a solution may introduce added complexity to the optimization problem, as it necessitates consideration of other constraints. Furthermore, the weight assignment criterion described above imparts dynamism to the weights in the cost function, making them more responsive to changes in network states and thereby enhancing the robustness of the cost function in the face of such variations.

D. LOW-LEVEL CONTROLLER: ACTUATION SYSTEM

As foreseen in the methodology section, the proposed control framework adheres to a hierarchical structure. Specifically, the upper and lower levels maintain communication as the MPC utilized at the upper level and the central command governing the actuation system are co-located within the Traffic Monitoring Center (TMC). Upon the establishment of regional split ratios by the MPC, it is assumed that this information is readily available within the actuation system, which is responsible for effectively coordinating each VMS panel to transfer routing suggestions to the network users. VMS are programmable traffic control devices that convey real-time information on network traffic conditions to drivers encountering them through the usage of LED panels installed on the roads. It is recognized that the VMS panels aim to influence driver routing decisions to enhance network performance. In this regard, they have a potential role in managing demand to match the capacity available, not only to alleviate acute problems caused by roadworks and accidents, but also to contribute to satisfactory performance of networks operating close to capacity over extended periods of high, but variable, demand [68].

In the context of our experiment, we define as SWPs the VMS-equipped roads. VMSs hold a strategic position in the

network because at these points vehicles can switch their path to an alternative one on the basis of the routing suggestion. Each SWP provides information concerning a specific target region, enabling vehicles to efficiently reach their intended destinations through an optimal sequence of crossing regions. Technically, SWPs display on their VMS panels the road (namely the Via road) selected as a reference for constraining the vehicle path through a specific crossing region. Indeed, in our experiment, the Via road represents a specific road located on the borders between two adjacent regions where vehicles can execute a regional crossing.

It is worth mentioning that the primary computational challenge for the low-level controller lies in selecting, for each of the SWPs, the most suitable Via road to be suggested. Clearly, the optimal Via roads are also chosen consistently with the optimal regional split ratio determined by the MPC. Specifically, the selection of the optimal Via road is guided by three conditions:

1 Identify less congested Via roads, considering their congestion index, such as the travel rate [69];
2 From the less congested Via roads associated with the SWP, choose the one closer to the current position of the SWP;
3 Display the selected Via on the VMS panel so that vehicles travelling through the destination can modify their route accordingly.

Once the information is displayed on the VMS panel, the vehicle can navigate toward its destination by entering the established crossing region. In doing so, the vehicle computes the optimal path for its final destination passing through the suggested Via road (the standard routing algorithm embedded in SUMO is used for this task). It is worth noting that leaving to each vehicle the effort of computing its actual path on the basis of the routing constraints reduces strongly to computational burden associated with the low-level controller. Furthermore, it is crucial to underscore that the setup of the VMS panels relies on the assumption of drivers' compliance when presented with route suggestions displayed on these panels. Notably, our primary focus in this study does not delve into the implications of driver compliance on the effectiveness of the dissemination of control actions among users.

Fig. 6 provides an example concerning the split of the traffic flow Q_{ij} destined for zone j from i into two distinct portions:

- Q_{ij}^h, representing the traffic flow that will traverse zone h en route to j.
- Q_{ij}^j, representing the traffic flow that will directly reach j without traversing h.

Aligned with the optimal splitting determined by the MPC, the actuation system advises individual users to navigate the neighboring crossing regions, denoted as h or j. This guidance is communicated through the display panel, indicating the appropriate Via roads. Crucially, the system ensures that the sum of Q_{ij}^h and Q_{ij}^j equals Q_{ij}.

FIGURE 6. Illustration of the possible splits between different zones.

TABLE 1. Scenario topology information, [66].

Area	$155.95km^2$	Intersections	4473
Total roads	$930.11km$	Traffic lights	203
Highways only	$88.79km$	Inductive loops	3157
Bus stops	561	Car Parks	175
Bus lines	38	Buildings	13553

III. NUMERICAL ANALYSIS

A. CASE STUDY

To test the proposed framework on a relevant and realistic case study, the whole city of Luxembourg has been chosen as a reference. The used scenario has been validated on real data [66], and is freely available in the microscopic traffic simulator SUMO.[3] Specifically, the simulation parameters utilized in [66] have been integrated into the traffic simulator to facilitate the case study. To achieve realistic traffic patterns in [66] the authors used the data published by the government, which is available on the Internet site of the Luxembourg National Institute of Statistics and Economic Studies (STATEC[4]) (e.g. population, age distribution) to generate the activity demand for the ACTIVITYGEN.[5] The used traffic demand is characterized by 300000 vehicles per day and it includes both transit and local traffic. A local vehicle has an origin, a destination, or both within the city. A vehicle in transit, on the other hand, has both its origin and its destination outside the city. The mobility model also includes public transport. The scenario covers a very extended area of almost $156km^2$ with $931km$ of road, to the authors' knowledge, the highest ever used to test this kind of application. Some information is summarized in Table 1, while Fig. 7 shows the network topology. Information has been retrieved from OpenStreetMap (OSM) and STATEC.

B. SIMULATION ENVIRONMENT

The simulation environment is generated by coupling various tools such as SUMO [65], Matrix Laboratory (MATLAB), and Optimization toolbox (OPTI).[6] SUMO is a microscopic traffic simulator and it emulates ground truth more

[3]https://github.com/lcodeca/LuSTScenario
[4]https://www.statistiques.public.lu
[5]http://sumo.dlr.de/wiki/ACTIVITYGEN
[6]https://github.com/jonathancurrie/OPTI

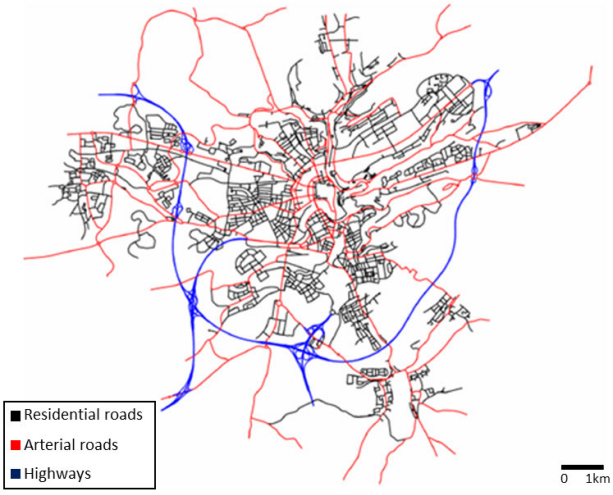

FIGURE 7. Luxembourg network topology, [66].

realistically. It supports online interaction with the MATLAB environment through the Traffic Control Interface (TraCI) regarded as TraCI4MATLAB [70]. The TraCI4MATLAB offers a high level of flexibility since it allows clients to insert and modify the objects inside the simulated environment as it operates in client-to-server scenarios.

Furthermore, SUMO guarantees the modeling of inter-modal traffic systems such as the contemporary simulation of private vehicles, public transportation systems, and pedestrians. It features support tools that are integrated to manage tasks such as route search, network import, display, and calculation of pollutant emissions. SUMO incorporates a set of tools to create and execute microscopic road traffic simulation scenarios, these tools are grouped into three categories:

- Mapping tools, to create the "map" (network).
- Traffic demand modeling tools.
- Simulation tools.

Moreover, the control strategy to be implemented in the proposed control framework is the MPC, which is based on the cyclic resolution of an optimization problem. In this regard, OPTI is used for the formalization of the optimization problem and its real-time resolution. OPTI is an open-source tool for the realization and resolution of linear, non-linear, continuous, and discrete optimization problems and can be easily integrated into the MATLAB simulation environment.

C. PRELIMINARY OPERATIONS

In order to apply the proposed routing scheme in Luxembourg some preliminary operations have been carried out. The first step has been zoning. Specifically, the city has been divided into different 9 regions as depicted in Fig. 8. Secondly, each region has been characterized by its own MFD and e-MFD curve. The MFD curves have been calibrated by following the fitting procedure proposed in [71] in which the authors create a confinement region through the intersection of linear lines (cuts) representing an upper bound of traffic states (uMFD). The MFD curve that emerges serves as a refined approximation of the minimum operator, that is called $soft-min$. An application example of this method is represented in Fig. 9 in which the fitted MFD of zone 4 is reported. It is worth noting that the weighted average flow of zone $\mathcal{I}$, $q^w_{\mathcal{I}}$, is calculated, consistently with [19], as:

$$q^w_{\mathcal{I}} = \frac{\sum_{i\in\mathcal{I}} q_i l_i}{\sum_{i\in\mathcal{I}} l_i} \tag{14}$$

in which l_i denotes the length of a road lane segment i belonging to the set of the lane of the zone $\mathcal{I}$ and q_i represents the flow measured by the corresponding detectors in a particular time slice. To construct the MFD curves, we computed the weighted average flow using data exclusively gathered from residential roads, while excluding arterial and highway segments from our dataset. This methodological approach aligns with prior research, acknowledging the distinct traffic dynamics observed on different road types [72]. Furthermore, when providing rerouting suggestions, we exclusively considered residential roads within the suggested paths.

The e-MFD curves were calibrated using the same fitting procedure outlined in [71], resulting in smooth approximations of the upper bound of emission levels (ue-MFD). It is noteworthy that the calibration of both MFD and e-MFD curves involved applying different perturbations to the original traffic demand provided by the application case study. This approach aimed to augment the quantity of data utilized during calibration, thereby enhancing its significance. Moreover, the same methodology was employed to estimate the quantities J_{1M} and J_{2M} in the cost function (8), which served to normalize the production and emission values estimated by the MFD and e-MFD curves.

However, the e-MFDs are non-linear curves, and make the optimization problem non-linear when used in the cost function (8) to estimate the CO_2 levels of the city centre. To overcome this issue, we decided to linearize them with piecewise linear functions (PWLFs), as depicted in Fig. 10, with reference to zone 1, in which the saturation branch of the e-MFD curve has been explored. The CO_2 emission levels of the region $\mathcal{I}$ are computed as:

$$CO_{2\mathcal{I}}(k) = \sum_{i\in\mathcal{I}} co_{2i}(k), \tag{15}$$

where $co_{2i}(k)$ represents the CO_2 emission value of the road segment i, belonging to the zone $\mathcal{I}$, at time instant k. The emissions relative to each road segment have been computed by using the model Handbook Emission Factors for Road Transport (HBEFA) v2.1[7] embedded in SUMO, which provides the data for each lane equipped with a detector. HBEFA is a standard data source for emission calculations in numerous studies[8] and other applications

[7]https://elib.dlr.de/89398/1/2ndGenEmissions.pdf
[8]https://www.hbefa.net/en/use-cases

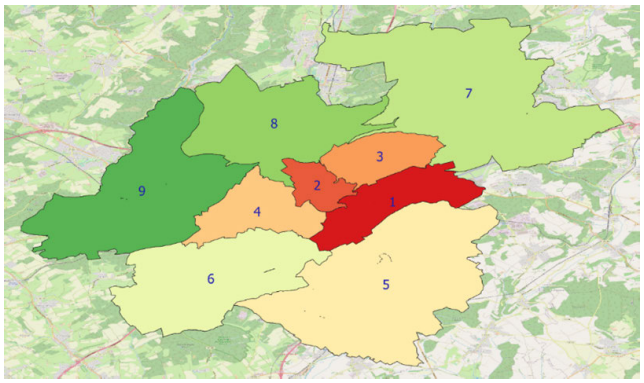

FIGURE 8. Luxembourg zoning.

TABLE 2. $RMSE_{\%}$ CO_2 estimated values.

Fitting Curve	ZONE 1	ZONE 2	ZONE 3	ZONE 4
Non-linear e-MFD	3.9	1.6	2	2.2
PWLF e-MFD	1.7	1.8	2	1.2

such as EcoTransIT World, IMMIS, TREMOD Transport Emission Model, and COPERT. It is the product of a common effort by funding agencies and development partners in six countries (i.e. Germany, Switzerland, Austria, Sweden, Norway, and France).

The CO_2 levels estimated by using both the PWLF and the non-linear e-MFD have been compared with the data measured in SUMO. Fig. 11 shows, for zone 4, the comparison between the estimated CO_2 levels, and the values measured in SUMO. The *RMSE* values, expressed in percentage, of each zone of the city centre have been reported In Table 2. Based on this analysis, it has been determined that employing PWLFs for estimating emission levels yields results comparable to those obtained using the nonlinear e-MFDs.

As already anticipated, the MPC control system is applied only in the city centre, i.e. the first 4 regions of Fig. 8, since these are the ones that usually get congested. However, in order to optimize the mobility performances of the city centre, the control acts on all the vehicles crossing the city centre, regardless of their origin and destination. It is worth noting that the modelling of a wider scenario with respect to the controlled part, allows us to evaluate the impact of the proposed methodology both outside the area of main interest (e.g. the whole city), and in the controlled part (e.g. the city centre); even in this case, to the authors' knowledge this kind of evaluation has been never carried out in literature in this kind of experiments.

The ultimate preliminary step, which involves the *SWPs* utilized to enact the control decisions of the MPC, has been completed. These points have been strategically positioned within each of the four controlled regions by carefully selecting roads that serve as bifurcations between two or more adjacent areas.

TABLE 3. Performed scenarios.

N_p	$thd = 0.6$	$thd = 0.7$	$thd = 0.8$
3	S_1	S_2	S_3
4	S_4	S_5	S_6
5	S_7	S_8	S_9
6	S_{10}	S_{11}	S_{12}
7	S_{13}	S_{14}	S_{15}

D. DESIGN OF EXPERIMENTS

In order to test the proposed methodology, different scenarios were prepared. In each scenario, the mobility and emission conditions of the network have been monitored for one day (24 hours) and data were aggregated for 300 second intervals; consistently the operating period of the MPC controller has been set to 5 *min* ($T_p = 300$ *sec*). The first scenario (S_0) is used for benchmarking and it does not include control (open-loop). It is used to evaluate the performances of the network without any control action, for successive comparison with the other scenarios. In other words, in S_0 the original demand provided in the application case study has been launched without the performed routing control scheme.

The first set of experiments is dedicated to the controller settings. In particular a set of simulations described in Table 3 has been prepared in order to find the best values for N_p and *thd*. In Table 3, 5 different scenarios correspond to a fixed value of *thd*, while the prediction horizon N_p varies between 3 and 7. These scenarios are used also to evaluate the computational burden of the MPC, quantified by means of the MPC feedback time FT_{MPC}, e.g. the execution time required to the MPC in one control time step to compute the optimal control sequence. The controller adopts, in all these cases, the multiobjective function introduced in the previous chapter. Once the best operating setting is established, a second set of experiments, corresponding to the simulation of scenarios $S_{\lambda 1}$, $S_{\lambda 2}$, and $S_{\lambda 3}$, has been performed, to evaluate the benefits of changing lambda each time step. Specifically, in $S_{\lambda 1}$, the weight λ inside the cost function (8) has been set to 0.8 in order to prioritize the minimization of the CO_2 levels. Conversely, in $S_{\lambda 2}$ the weight has been set to 0.2 and finally in $S_{\lambda 3}$ the two terms of the cost function (8) have been weighted with the same value by choosing $\lambda = 0.5$. Finally, the scenarios S_{SUMO}, S_{CO2}, and S_{PR}, have been performed, with the objective of evaluating the advantages of the proposed approach with respect to simpler ones and demonstrate its robustness. Specifically, in the S_{SUMO} scenario, the routing suggestions at SWPs are based on the default (Dijkstra) re-routing algorithm implemented in SUMO [73], then the system is not performing any network optimization, but the suggestion only minimizes each user travel time. Scenarios S_{CO2} and S_{PR} implement the reference controlling framework but with the single objective of minimizing emissions, and maximizing traffic throughput respectively. These three additional scenarios have been

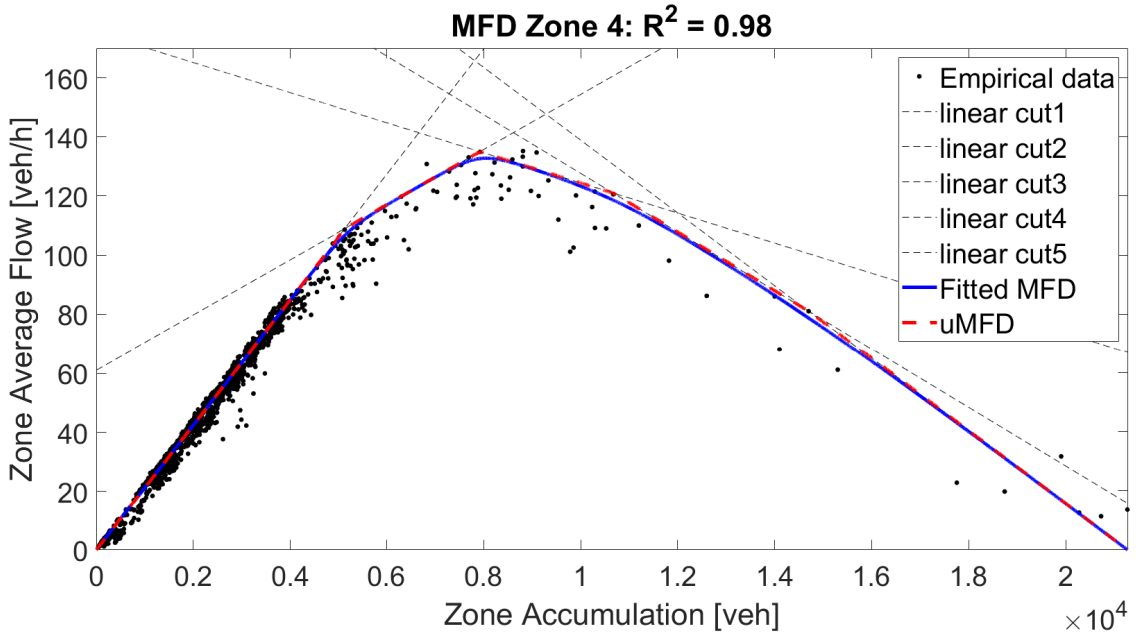

FIGURE 9. Zone 4 MFD calibration.

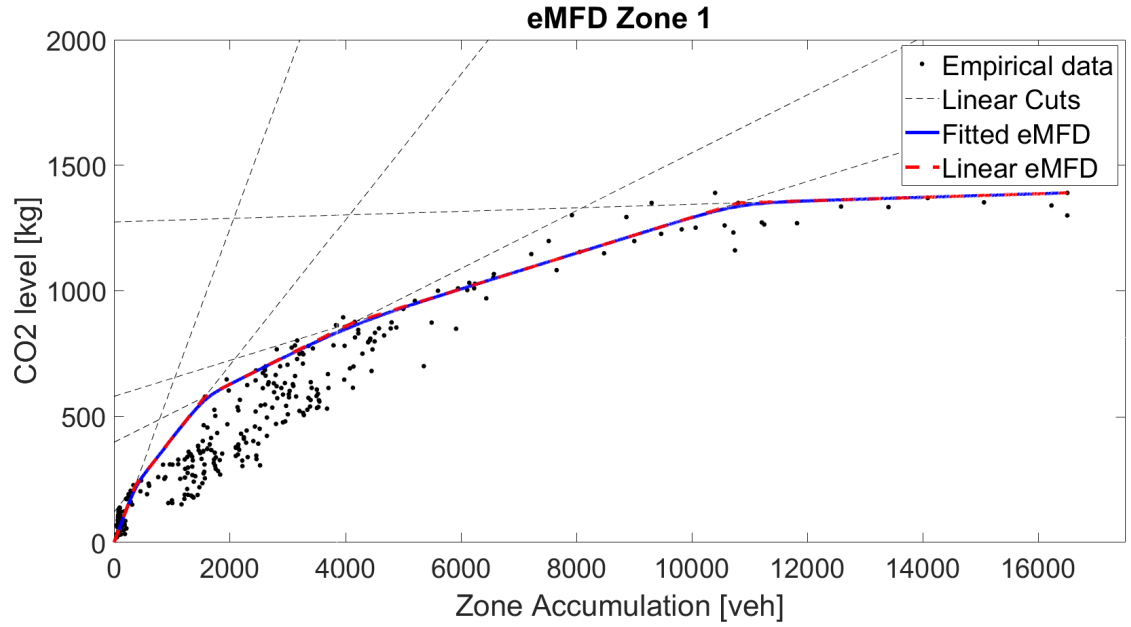

FIGURE 10. Zone 1 e-MFD calibration.

compared with the best-performing scenario of the tuning activity that has been used as a benchmark in the comparison. In total, 21 different scenarios have been developed, and each of them has been run using 3 different computer machines and 3 different seed values of the traffic simulator SUMO [65]. Therefore, 189 simulations have been run globally, 9 for each scenario, in order to increase the significance of the results. In all simulations in which the controller is activated (closed-loop), in any form, its action starts when the congestion in the city centre occurs (MPC activation condition) and it is disabled when congestion ends so that the MPC action is event-based (conditional MPC). This means that the vehicles in the simulation stick to the path they were previously assigned by the controller when the activation condition of the MPC is not satisfied, while the new vehicle inserted in the simulation follows the original path assignment provided by default by the original traffic demand of the application case study.

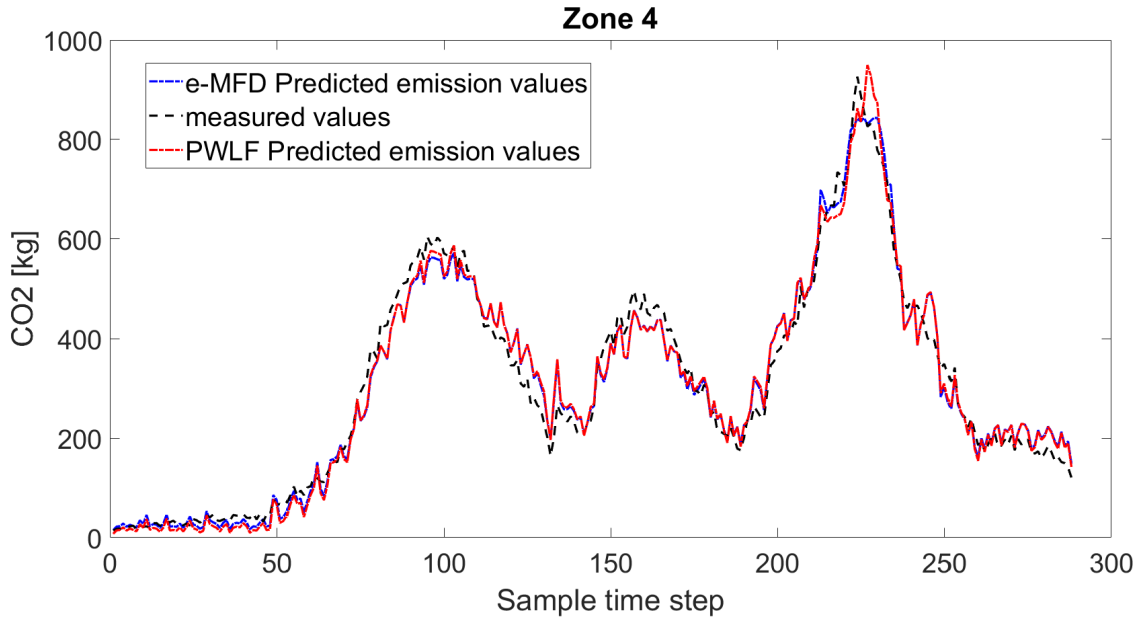

FIGURE 11. Zone 4 estimated CO_2 levels.

E. KEY PERFORMANCE INDEXES

Two Key Performance Indexes (KPIs) are defined in order to quantify the congestion level of each zone, $s_{i\%}$ and Δ_i. The indicator $s_{i\%}$ quantifies the level of congestion in a zone in terms of the difference between the zone i maximum accumulation value and the zone i critical value, expressed in percentage. While Δ_i simply represents the time window in which the accumulation in the zone i exceeds the critical value. In Fig. 12 from the zone i accumulation trend in time, it is possible to mark the $s_{i\%}$ and Δ_i values. The KPI $s_{i\%}$ expression is the following:

$$s_{i\%} = \frac{n_{peak,i} - n_{cr,i}}{n_{cr,i}} \cdot 100, \tag{16}$$

where $n_{peak,i}$ represents the zone i peak accumulation value and $n_{cr,i}$ the critical value of the zone. The KPI Δ_i, by looking the Fig. 12, is simply calculated as:

$$\Delta_i = t_2 - t_1, \tag{17}$$

where t_1 represents the time instant in which the congestion occurs in zone i and t_2 is the time instant in which the congestion ends. The aggregation of the peak accumulation value and the associated Δ value of each zone provides a third metric, here defined as congestion severity CS $[veh \cdot h]$ of the city centre, that it is represented as follows:

$$CS = \sum_{i \in \mathcal{N}_c} n_{peak,i} \cdot \Delta_i, \tag{18}$$

where the Δ_i value of each zone i is expressed in hours and $\mathcal{N}_c = [1, 2, 3, 4]$ represents the city center zones set.

Apart from these quantitative KPIs, the time evolutions of each zone CO_2 emission level and travel Production, and the empirical MFDs, are used to give a qualitative evaluation of the controller effects. In particular, the network CO_2 emission level and travel Production values have been further taken into account in order to qualitatively analyze the global impact of the proposed control framework on the whole network. These quantities have been calculated by extending the Eqs (14) and (15) from zone to network level, including in the formulas each link of the network.

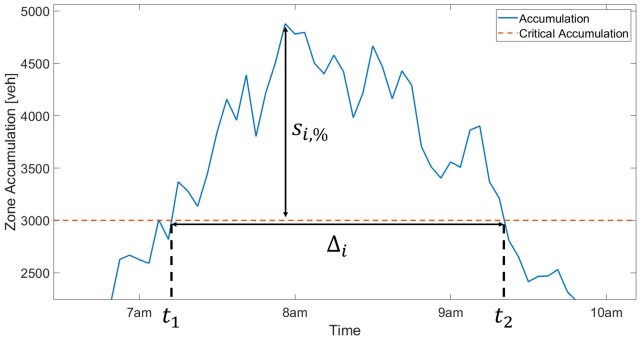

FIGURE 12. Quantitative KPIs representation.

IV. RESULTS AND DISCUSSION

In this section, three different categories of results are presented. Firstly, activities carried out for tuning the *thd* value used in the multiobjective cost function weight assignment criterion are introduced. The second results category concerns the comparison of the proposed control framework, where the optimal *thd* tuning is set on the basis of the previous, with other control strategies. Finally, the analysis of the effects of the multiobjective MPC on the whole network, namely the global effects of the multiobjective MPC, are introduced and discussed.

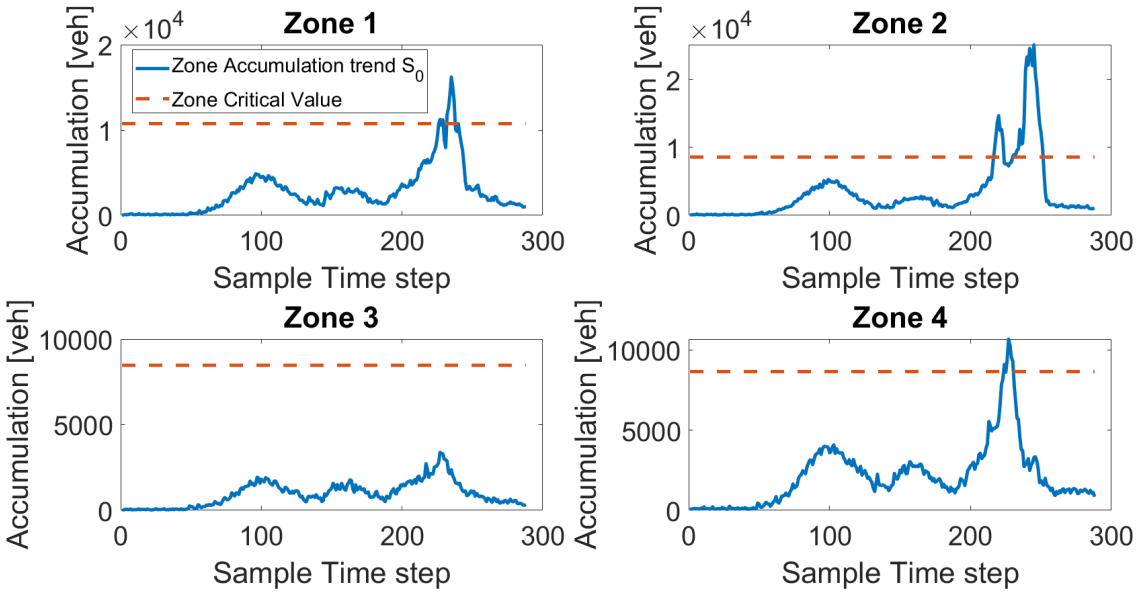

FIGURE 13. Congestion levels of S_0 scenario.

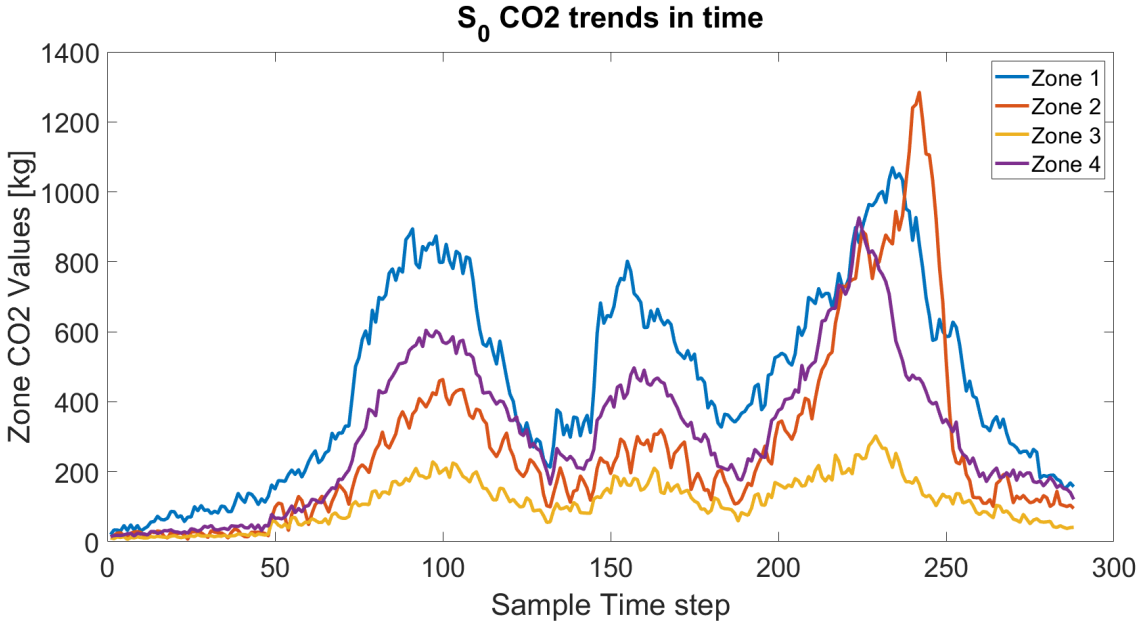

FIGURE 14. CO_2 levels of S_0 scenario.

A. TUNING ACTIVITY RESULTS

A preliminary step for any tuning activity is the definition of a reference and of some KPIs. To do that, in this case, the congestion and CO_2 emission levels of the city centre in the open-loop scenario S_0 have been measured. The congestion levels of the city centre are detected for each zone by monitoring accumulation trends in time. Fig. 13 reports the values for the whole day for zones 1-4, and also looking at it qualitatively it is clear that zone 3 is the only one zone where the accumulation never exceeds the critical value. For this reason, the KPIs chosen for evaluating congestion levels, $s_{\%}$ and Δ, have been not reported in Table 4 for zone 3. Fig. 14 presents the time series of the CO_2 emission values of the zones 1-4. Consistently, the CO_2 emission levels related to the zone 3 are significantly lower w.r.t. the other zones of the city centre. On the basis of the previous, zone 3 has been excluded from the analysis both in S_0 and in any further scenario.

To evaluate the improvement introduced by the M-MPC activation, the scenarios of Table 3 have been performed. Results of the KPIs associated with these scenarios are

reported in Fig. 15 where each curve has a fixed value of the parameter *thd*, used in the real-time cost function (8) weight computation, and the values of the congestion severity *CS* vary on the basis of the different prediction horizons N_p used in the MPC framework. It is worth noting that each curve has a decreasing trend with the increase of N_p since a greater value of the prediction horizon allows the MPC to have a wider optimization time window. Furthermore, the curve with the value of *thd* fixed to 0.6 leads to better mitigation of the congestion volume of the city centre. We remind that in this case, the MPC tries to set the cost function weight in order to guarantee in the city centre of Luxembourg, at the same time, CO_2 emission levels not greater than the 60% of the maximum value and Travel Production values at least equal to the 60% of the maximum value. On the basis of that, in the *thd* calibration activity values of *thd* lower than 0.6 have been investigated, but they do not guarantee any significant improvement in terms of city centre *CS*. For this reason, 0.6 has been finally chosen as the optimal operating value. For the sake of clarity, the values of $s_{\%}$ and Δ, related to each zone in each performed scenario have been reported in Table 4. It is clear that the optimal setting of the controller parameters relies on the Scenario S_{13}, at which the lowest value of *CS* is reached. However, each closed loop scenario leads to an improvement in terms of $s_{\%}$ and Δ w.r.t. the open loop scenario S_0. This aspect demonstrates the robustness of the controller towards parameter changes.

In Table 4 each scenario is also characterized by the average value of the MPC Feedback time during the whole MPC operation time window $\widehat{FT_{MPC}}$ $[ms]$. It is worth noting that also in the heaviest cases, where the N_p is set to the greatest value (i.e. 7 control time steps of prediction) and the optimization problem is made up of 294 variables, 183 constraints and 224 bounds, the Feedback time of the MPC remains lower than $1sec$, and its average value still remains in the order of the milliseconds. Of course, the performance of the tool could be further improved by means of specific hardware/software solutions, however on the basis of this result we conclude that this control scheme is able to work in a real-time application.

There are some important aspects associated with the optimal setting of the prediction horizon N_p. On one hand, the prediction horizon should be comparable to the time needed to travel through a region network. In this regard, a much shorter horizon may lead to "myopic" control actions [74]. On the other hand, theoretically speaking, the usage of a smaller prediction horizon could lead to a more accurate estimation of the region accumulation state variables in the forecasting procedure. But this latter aspect is strongly sharpened by the operating frequency of the MPC since the impact of the model inaccuracies on the quality of the traffic variables prediction is strongly reduced. Indeed the real-time feedback allows for frequent updates on the control strategy decisions on the basis of the current measurement of network traffic states. In summary, the optimal operating value of the prediction horizon ($N_p = 7$) seems to be a good compromise between performance sensitivity with respect to inaccuracies of the traffic parameters and myopic control actions.

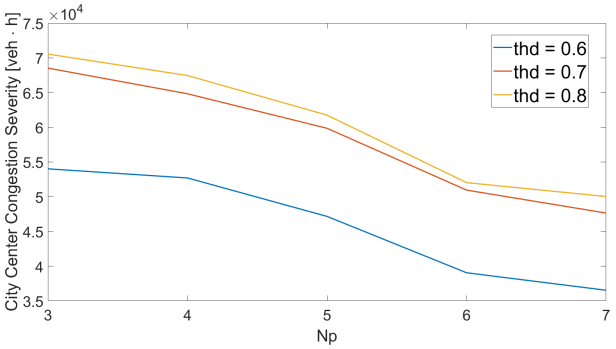

FIGURE 15. City center congestion severity with different values of the controller parameters.

TABLE 4. Local KPIs of the scenarios in the tuning activity.

Scenarios	$\widehat{FT_{MPC}}[ms]$	Zone 1		Zone 2		Zone 4	
		$s_{\%}$	$\Delta[min]$	$s_{\%}$	$\Delta[min]$	$s_{\%}$	$\Delta[min]$
S_0	-	51	35	193	180	23	40
S_2	52.34	19.16	5	151.09	170	26.03	35
S_3	44.17	29.27	5	162.10	170	16.05	5
S_4	98.26	24.40	10	123.65	155	6.33	5
S_5	97.12	25.18	10	127.04	175	20.14	20
S_6	95.89	32.45	20	146.66	170	20.15	15
S_7	129.78	-4.24	0	109.37	155	9.06	5
S_8	132.43	-3.65	0	116.77	180	9.04	25
S_9	130.49	1.23	5	115.38	190	9.03	15
S_{10}	179.36	-1.76	0	97.90	135	7.75	5
S_{11}	182.19	-10.51	0	129.78	150	7.75	10
S_{12}	185.73	-10.51	0	134.78	150	7.75	10
S_{13}	217.25	**-1.76**	**0**	**89.30**	**135**	**7.75**	**5**
S_{14}	220.37	-0.15	0	107.78	160	7.75	5
S_{15}	215.43	-0.15	0	114.90	160	7.75	5

TABLE 5. Local KPIs of the scenarios in the comparison activity.

Scenarios	Zone 1		Zone 2		Zone 4	
	$s_{\%}$	$\Delta[min]$	$s_{\%}$	$\Delta[min]$	$s_{\%}$	$\Delta[min]$
S_0	51	35	193	180	23	40
$S_{\lambda 1}$	12.76	15	110.32	170	13.95	10
$S_{\lambda 2}$	0.01	0	92.96	140	9.54	5
$S_{\lambda 3}$	2.23	5	94.42	145	11.75	5
S_{SUMO}	25.96	30	127.56	160	9.41	30
S_{CO2}	26.35	20	112.41	170	15.00	15
S_{PR}	3.49	5	93.80	165	9.94	10
S_{13}	**-1.76**	**0**	**89.30**	**135**	**7.75**	**5**

B. COMPARISON OF THE PROPOSED CONTROL FRAMEWORK WITH OTHER CONTROL STRATEGIES

The reference optimal performing scenario (S_{13}) has been benchmarked with $S_{\lambda 1}$, $S_{\lambda 2}$, and $S_{\lambda 3}$. In this regard in Table 5 the values of $s_{\%}$ and Δ have been reported in order to quantify the congestion levels of these scenarios. In Fig. 16 the CO_2 levels of S_{13} have been compared with the CO_2 levels of $S_{\lambda 1}$, $S_{\lambda 2}$, and $S_{\lambda 3}$. The data presented in Table 5 clearly shows that scenarios $S_{\lambda 2}$, and $S_{\lambda 3}$ offer superior congestion mitigation compared to $S_{\lambda 1}$ in which the value of the weight λ has been set in order to prioritize the minimization of the city centre CO_2 levels. Despite this, the scenario S_{13} still outperforms others in terms of congestion mitigation. Conversely, in Fig. 16 the CO_2 values registered in $S_{\lambda 1}$ are

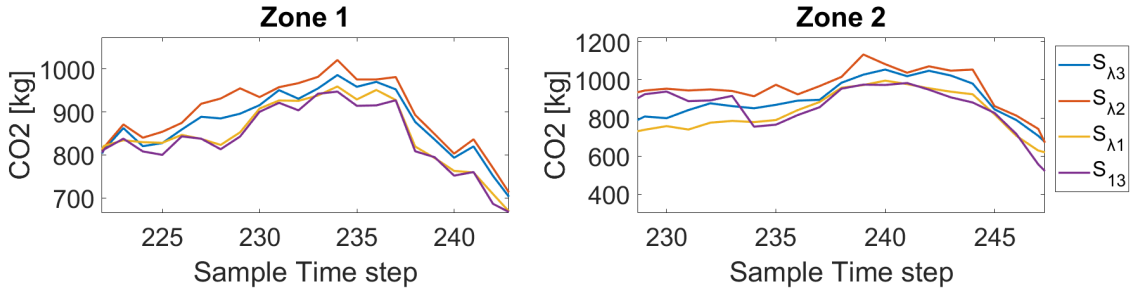

FIGURE 16. Zones 1 and 2 CO_2 values.

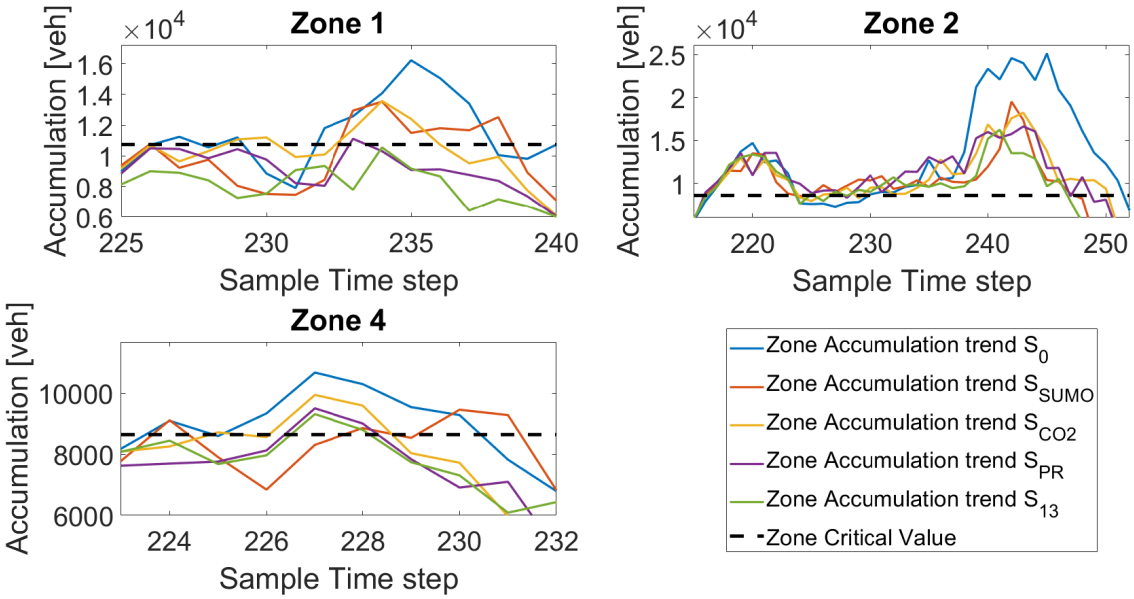

FIGURE 17. City center zones accumulation values.

lower than those in $S_{\lambda 2}$ and $S_{\lambda 3}$. Notably, the CO_2 levels observed in $S_{\lambda 1}$ align with those in S_{13}. These findings highlight the advantages of dynamically adjusting the weight λ in real-time, as opposed to using a constant value.

Finally, the benchmarking scenario S_{13} has been compared with 3 alternative (and simpler) control strategies represented by the scenarios S_{SUMO}, S_{CO2} and S_{PR}; as a reference, also the open-loop scenario S_0 is considered in the comparison. Consistently with others, the Dijkstra re-routing algorithm of the scenario S_{SUMO} is enabled from 6 pm to 8 pm representing the critical time window in which the congestion occurs in the scenario. Also the characterizations of scenarios S_{CO2} and S_{PR} are totally consistent with those presented in the previous section. The only difference concerns the objective function (8), where the value of the weight λ is fixed to 1 and 0, respectively in the scenarios S_{CO2} and S_{PR}, in order to isolate the effect of minimizing CO_2 emissions or maximizing Production for the whole MPC operating time.

Accumulation values of zones 1, 2 and 4 observed in each scenario are depicted in Figure 17; the values are reported with a focus on the time window in which the control scheme operates. It could be noted that all the routing strategies allow congestion mitigation of the city centre zones wrt S_0 scenario. The developed control scheme in S_{13} reaches better performances in terms of congestion mitigation, especially in Zone 1. The S_{PR} shows a performance totally consistent with S_{13}, while the routing systems of S_{SUMO} and S_{CO2} are not able to completely delete the congestion. Also, the values of $s_{\%}$ and Δ associated with these scenarios, reported in Table 5, confirm the qualitative analysis of Figure 17.

Subsequently, CO_2 levels in zones 1,2, and 4 are compared in Figure 18. This time, emission levels of the city centre regions w.r.t. the open-loop scenario are not significantly reduced in the scenarios S_{SUMO} and S_{PR}. This was totally expected since the Dijkstra routing algorithm of SUMO does not take explicitly into account the CO_2 emission levels of the city, and similarly happens for the objective functions of the MPC developed in S_{PR}. Conversely, the controller shows its best performances in S_{CO2} where the

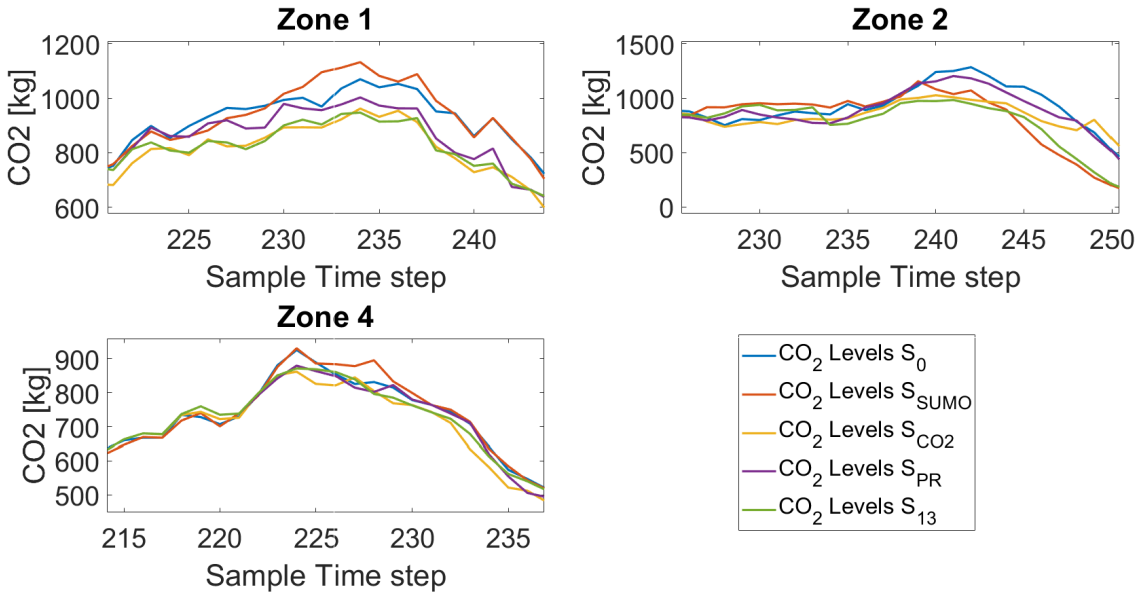

FIGURE 18. City center zones CO_2 values.

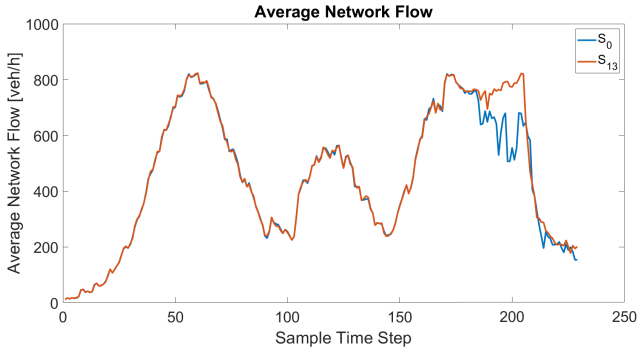

FIGURE 19. Global results of scenarios S_0 and S_{13}: Average network flow.

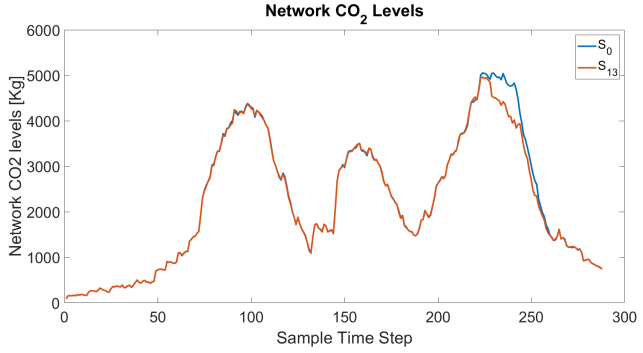

FIGURE 20. Global results of scenarios S_0 and S_{13}: CO_2 network levels.

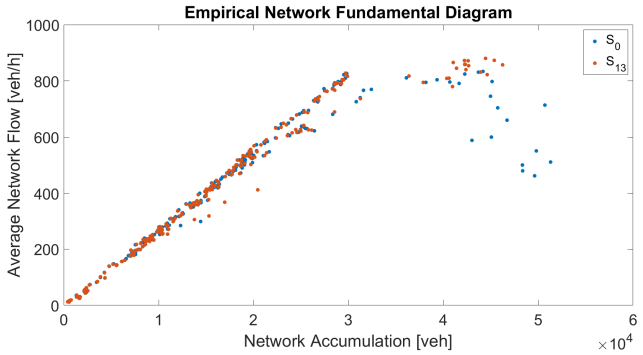

FIGURE 21. Global results of scenarios S_0 and S_{13}: Empirical network fundamental diagrams.

CO_2 emissions are reduced wrt S_0 on average of 14%, 12% and 4% in zone 1, 2 and 4 respectively. It is worth noting that the performances of the controller in the scenario S_{13} are consistent with those in S_{CO2}. Considering all together, it can be affirmed that the proposed M-MPC is able to deal with both congestion and emission levels in the city centre of Luxembourg and allows finding a good compromise between the two conflicting aspects.

C. GLOBAL EFFECTS OF THE PROPOSED CONTROLLER

The evaluation of the effects of the proposed control scheme on the whole city of Luxembourg has been carried out by considering both congestion and CO_2 emissions. Of course, the two aspects are here evaluated by defining a unique measure for the whole network. In this regard, in Figures 19, 20 and 21, the Empirical Network Fundamental Diagram, the time series of the Average Network Flow, and the time series of the Network CO_2 emissions of the scenarios S_0 and S_{13} have been compared respectively. The analysis of the figures confirms that even if the MPC controls only the vehicles that have to cross the city centre, it alters the mobility and emission performances of the whole network. In particular, the best-performing controller in the scenario S_{13} allows an increment of the 17.7% of the average network flow while reducing network level CO_2 emission by 8%. The empirical network fundamental diagram related to scenario S_{13} confirms that the network, differently from scenario S_0, does not operate in the congested regime, but in the saturation

one in which the Average Network Flow is maximized and the behaviour of the network is optimized.

V. CONCLUSION AND FUTURE DEVELOPMENTS

In this work, a Multiobjective Model Predictive Control has been developed in order to mitigate both congestion and CO_2 emission levels in an urban network. The proposed approach has been tested on the realistic and challenging scenario represented by the whole network of the city of Luxembourg. The paradigm of MFD has been used for traffic dynamics modelling efficiently, while the e-MFDs curves have been used to compute the CO_2 aggregated emission levels of the urban network. A tuning activity of the controller parameters N_p and *thd* has been carried out, in order to test the robustness of the MPC towards different values of the operating parameters and select the best-performing parameter settings. The results of the tuning activity show that the proposed framework is generally able to improve the network performances (with each parameter setting).

The best-performing controller has been compared with a naive approach based on the activation of the routing algorithm embedded in SUMO. Apart from that, the multiobjective approach has been compared with 2 simpler single-objective versions of the controller. The congestion is related to the emissions so it is expected that by reducing the congestion levels of a network a decrease of CO_2 emission levels consequently appears. Unfortunately, this is not so obvious. Indeed, the routing algorithm implemented in the scenario S_{SUMO} is able to reduce the congestion levels, but it does not guarantee a significant decrease in the CO_2 emission levels. The usage of a multiobjective cost function in the MPC framework allows us to find a good compromise between congestion and emission mitigation. By means of scenarios S_{PR} and S_{CO2} we demonstrated that this is not guaranteed by modelling separately the 2 aspects in the cost function.

More interestingly, the multiobjective controller reduces simultaneously congestion and emissions levels in the city center, but it also impacts strongly on the global network by allowing an increment of the 17.7% of the average network flow and reducing network CO_2 emissions by 8%.

As a future development, other pollutant emission levels could be taken into account inside the multiobjective cost function in the MPC framework. There is a need for further investigation into the economic costs and potential social challenges related to the adoption of the proposed M-MPC strategy, as well as strategies for effective communication and implementation with the public. This involves analyzing financial implications, including setup and maintenance costs and potential savings. Addressing social challenges requires engaging stakeholders to mitigate community impacts and equity concerns. Effective communication strategies are crucial, requiring clear materials and engagement across channels. A well-defined implementation plan is vital, delineating milestones for seamless coordination among stakeholders in deploying the proposed M-MPC strategy. Besides, the advent of automated vehicles will also leverage advanced traffic management solutions (such as MPC based control) soon [75], [76].

REFERENCES

[1] C. Brosilow and B. Joseph, *Techniques of Model-Based Control*. Upper Saddle River, NJ, USA: Prentice-Hall, 2002.
[2] V. Mauro and C. Di Taranto, "UTOPIA," *IFAC Proc.*, vol. 23, no. 2, pp. 245–252, 1990.
[3] N. Gartner, J. Little, and H. Gabbay, "MITROP: A computer program for simultaneous optimisation of offsets, splits and cycle time," *Traffic Eng. Control*, vol. 17, nos. 8–9, pp. 355–359, 1976.
[4] N. H. Gartner, F. J. Pooran, and C. M. Andrews, "Implementation of the OPAC adaptive control strategy in a traffic signal network," in *Proc. IEEE Intell. Transp. Syst.*, Aug. 2001, pp. 195–200.
[5] J. J. Henry, J. L. Farges, and J. Tuffal, "The prodyn real time traffic algorithm," *IFAC Proc. Volumes*, vol. 16, no. 4, pp. 305–310, Apr. 1983.
[6] P. Mirchandani and F.-Y. Wang, "RHODES to intelligent transportation systems," *IEEE Intell. Syst.*, vol. 20, no. 1, pp. 10–15, Jan. 2005.
[7] F. Boillot, J. Blosseville, J. Lesort, V. Motyka, M. Papageorgiou, and S. Sellam, "Optimal signal control of urban traffic networks," in *Proc. Road Traffic Monitoring*, 1992, p. 75.
[8] C. Bielefeldt, "MOTION—A new on-line traffic signal network control system motion," in *Proc. 7th Int. Conf. 'Road Traffic Monitor. Control'*, 1994, pp. 55–59.
[9] P. Lowrie, "The Sydney co-ordinated adaptive traffic system: Principles, methodology, algorithms," in *Proc. Int. Conf. Road Traffic Signalling*, 1982, pp. 67–70.
[10] D. I. Robertson and R. D. Bretherton, "Optimizing networks of traffic signals in real time–The SCOOT method," *IEEE Trans. Veh. Technol.*, vol. 40, no. 1, pp. 11–15, Feb. 1991.
[11] Y. Li, R. Mohajerpoor, and M. Ramezani, "Perimeter control with real-time location-varying cordon," *Transp. Res. B, Methodol.*, vol. 150, pp. 101–120, Aug. 2021.
[12] A. Kouvelas, M. Saeedmanesh, and N. Geroliminis, "A linear formulation for model predictive perimeter traffic control in cities," *IFAC-PapersOnLine*, vol. 50, no. 1, pp. 8543–8548, 2017.
[13] M. Yildirimoglu, I. I. Sirmatel, and N. Geroliminis, "Hierarchical control of heterogeneous large-scale urban road networks via path assignment and regional route guidance," *Transp. Res. B, Methodol.*, vol. 118, pp. 106–123, Dec. 2018.
[14] Y. Ren, Z. Hou, I. I. Sirmatel, and N. Geroliminis, "Data driven model free adaptive iterative learning perimeter control for large-scale urban road networks," *Transp. Res. C, Emerg. Technol.*, vol. 115, Jun. 2020, Art. no. 102618.
[15] N. Moshahedi, L. Kattan, and R. Tay, "A network-wide anticipatory control of an urban network using macroscopic fundamental diagram," *Transportmetrica B, Transp. Dyn.*, vol. 9, no. 1, pp. 415–436, Jan. 2021.
[16] M. Hajiahmadi, V. L. Knoop, B. De Schutter, and H. Hellendoorn, "Optimal dynamic route guidance: A model predictive approach using the macroscopic fundamental diagram," in *Proc. 16th Int. IEEE Conf. Intell. Transp. Syst. (ITSC)*, Oct. 2013, pp. 1022–1028.
[17] M. Hajiahmadi, B. De Schutter, and H. Hellendoorn, "Model predictive traffic control: A mixed-logical dynamic approach based on the link transmission model," *IFAC Proc. Volumes*, vol. 45, no. 24, pp. 144–149, Sep. 2012.
[18] G. S. van de Weg, M. Keyvan-Ekbatani, A. Hegyi, and S. P. Hoogendoorn, "Linear MPC-based urban traffic control using the link transmission model," *IEEE Trans. Intell. Transp. Syst.*, vol. 21, no. 10, pp. 4133–4148, Oct. 2020.
[19] N. Geroliminis and C. F. Daganzo, "Existence of urban-scale macroscopic fundamental diagrams: Some experimental findings," *Transp. Res. B., Methodol.*, vol. 42, no. 9, pp. 759–770, Nov. 2008.
[20] B. Wei and D. Sun, "A two-layer network dynamic congestion pricing based on macroscopic fundamental diagram," *J. Adv. Transp.*, vol. 2018, pp. 1–11, Aug. 2018.
[21] H. Fu, S. Chen, K. Chen, A. Kouvelas, and N. Geroliminis, "Perimeter control and route guidance of multi-region MFD systems with boundary queues using colored Petri nets," *IEEE Trans. Intell. Transp. Syst.*, vol. 23, no. 8, pp. 12977–12999, Aug. 2022.

[22] A. Genser and A. Kouvelas, "Dynamic optimal congestion pricing in multi-region urban networks by application of a multi-layer-neural network," *Transp. Res. C, Emerg. Technol.*, vol. 134, Jan. 2022, Art. no. 103485.

[23] K. Aboudolas and N. Geroliminis, "Perimeter and boundary flow control in multi-reservoir heterogeneous networks," *Transp. Res. B, Methodol.*, vol. 55, pp. 265–281, Sep. 2013.

[24] M. Ramezani, J. Haddad, and N. Geroliminis, "Dynamics of heterogeneity in urban networks: Aggregated traffic modeling and hierarchical control," *Transp. Res. B, Methodol.*, vol. 74, pp. 1–19, Apr. 2015.

[25] J. M. Maciejowski, *Predictive Control: With Constraints*. London, U.K.: Pearson Education, 2002.

[26] J. Nocedal and S. J. Wright, *Numerical Optimization*. Springer, 1999.

[27] N. Geroliminis, J. Haddad, and M. Ramezani, "Optimal perimeter control for two urban regions with macroscopic fundamental diagrams: A model predictive approach," *IEEE Trans. Intell. Transp. Syst.*, vol. 14, no. 1, pp. 348–359, Mar. 2013.

[28] R. X. Zhong, C. Chen, Y. P. Huang, A. Sumalee, W. H. K. Lam, and D. B. Xu, "Robust perimeter control for two urban regions with macroscopic fundamental diagrams: A control-Lyapunov function approach," *Transp. Res. Procedia*, vol. 23, pp. 922–941, 2017.

[29] T. Lei, Z. Hou, and Y. Ren, "Data-driven model free adaptive perimeter control for multi-region urban traffic networks with route choice," *IEEE Trans. Intell. Transp. Syst.*, vol. 21, no. 7, pp. 2894–2905, Jul. 2020.

[30] Q. Guo and X. Ban, "Macroscopic fundamental diagram based perimeter control considering dynamic user equilibrium," *Transp. Res. B, Methodol.*, vol. 136, pp. 87–109, Jun. 2020.

[31] J. Haddad and Z. Zheng, "Adaptive perimeter control for multi-region accumulation-based models with state delays," *Transp. Res. B, Methodol.*, vol. 137, pp. 133–153, Jul. 2020.

[32] M. Keyvan-Ekbatani, R. C. Carlson, V. L. Knoop, and M. Papageorgiou, "Optimizing distribution of metered traffic flow in perimeter control: Queue and delay balancing approaches," *Control Eng. Pract.*, vol. 110, May 2021, Art. no. 104762.

[33] C. Chen, Y. P. Huang, W. H. K. Lam, T. L. Pan, S. C. Hsu, A. Sumalee, and R. X. Zhong, "Data efficient reinforcement learning and adaptive optimal perimeter control of network traffic dynamics," *Transp. Res. C, Emerg. Technol.*, vol. 142, Sep. 2022, Art. no. 103759.

[34] J. Yuan, C. Wu, K. L. Teo, S. Zhao, and L. Meng, "Perimeter control with state-dependent delays: Optimal control model and computational method," *IEEE Trans. Intell. Transp. Syst.*, vol. 23, no. 11, pp. 20614–20627, Nov. 2022.

[35] T. Dantsuji, Y. Takayama, and D. Fukuda, "Perimeter control in a mixed bimodal bathtub model," *Transp. Res. B, Methodol.*, vol. 173, pp. 267–291, Jul. 2023.

[36] N. Moshahedi and L. Kattan, "Alpha-fair large-scale urban network control: A perimeter control based on a macroscopic fundamental diagram," *Transp. Res. C, Emerg. Technol.*, vol. 146, Jan. 2023, Art. no. 103961.

[37] M. Rahmani, E. Jenelius, and H. N. Koutsopoulos, "Non-parametric estimation of route travel time distributions from low-frequency floating car data," *Transp. Res. C, Emerg. Technol.*, vol. 58, pp. 343–362, Sep. 2015.

[38] T. Erdelić, T. Carić, M. Erdelić, L. Tišljarić, A. Turković, and N. Jelušić, "Estimating congestion zones and travel time indexes based on the floating car data," *Comput., Environ. Urban Syst.*, vol. 87, May 2021, Art. no. 101604.

[39] J. W. Wedel, B. Schünemann, and I. Radusch, "V2X-based traffic congestion recognition and avoidance," in *Proc. 10th Int. Symp. Pervasive Syst., Algorithms, Netw.*, Dec. 2009, pp. 637–641.

[40] P. Wang, H. Deng, J. Zhang, and M. Zhang, "Real-time urban regional route planning model for connected vehicles based on V2X communication," *J. Transp. Land Use*, vol. 13, no. 1, pp. 517–538, Nov. 2020.

[41] S. Scherler, S. Jacobitz, X. Liu-Henke, and M. Henke, "Cloud-based V2X communication for dynamic intelligent guidance in connected traffic systems," in *Proc. IEEE Int. Symp. Syst. Eng. (ISSE)*, Sep. 2021, pp. 1–7.

[42] M. Khanjary and S. M. Hashemi, "Route guidance systems: Review and classification," in *Proc. 6th Euro Amer. Conf. Telematics Inf. Syst. (EATIS)*, May 2012, pp. 1–7.

[43] M. Botte, L. Pariota, L. D'Acierno, and G. N. Bifulco, "An overview of cooperative driving in the European union: Policies and practices," *Electronics*, vol. 8, no. 6, p. 616, May 2019.

[44] M. Hajiahmadi, J. Haddad, B. De Schutter, and N. Geroliminis, "Optimal hybrid macroscopic traffic control for urban regions: Perimeter and switching signal plans controllers," in *Proc. Eur. Control Conf. (ECC)*, Jul. 2013, pp. 3500–3505.

[45] I. I. Sirmatel and N. Geroliminis, "Economic model predictive control of large-scale urban road networks via perimeter control and regional route guidance," *IEEE Trans. Intell. Transp. Syst.*, vol. 19, no. 4, pp. 1112–1121, Apr. 2018.

[46] M. Yildirimoglu, M. Ramezani, and N. Geroliminis, "Equilibrium analysis and route guidance in large-scale networks with MFD dynamics," *Transp. Res. Proc.*, vol. 9, pp. 185–204, Jan. 2015.

[47] V. L. Knoop, S. Hoogendoorn, and J. Van Lint, "The impact of traffic dynamics on macroscopic fundamental diagram," in *Proc. 92nd Annu. Meeting Transp. Res. Board*, Washington, DC, USA, Jan. 2013, pp. 13–17.

[48] H. S. Mahmassani, M. Saberi, and A. Zockaie, "Urban network gridlock: Theory, characteristics, and dynamics," *Proc. Social Behav. Sci.*, vol. 80, pp. 79–98, Jun. 2013.

[49] V. V. Gayah and C. F. Daganzo, "Clockwise hysteresis loops in the macroscopic fundamental diagram: An effect of network instability," *Transp. Res. B, Methodol.*, vol. 45, no. 4, pp. 643–655, May 2011.

[50] A. Mazloumian, N. Geroliminis, and D. Helbing, "The spatial variability of vehicle densities as determinant of urban network capacity," *Phil. Trans. Roy. Soc. A, Math., Phys. Eng. Sci.*, vol. 368, no. 1928, pp. 4627–4647, Oct. 2010.

[51] A. Loder, L. Ambühl, M. Menendez, and K. W. Axhausen, "Understanding traffic capacity of urban networks," *Sci. Rep.*, vol. 9, no. 1, p. 16283, Nov. 2019.

[52] M. A. Silgu, I. G. Erdagi, G. Göksu, and H. B. Celikoglu, "Combined control of freeway traffic involving cooperative adaptive cruise controlled and human driven vehicles using feedback control through SUMO," *IEEE Trans. Intell. Transp. Syst.*, vol. 23, no. 8, pp. 11011–11025, Aug. 2022.

[53] P. Fernandes and U. Nunes, "Platooning of autonomous vehicles with intervehicle communications in SUMO traffic simulator," in *Proc. 13th Int. IEEE Conf. Intell. Transp. Syst.*, Sep. 2010, pp. 1313–1318.

[54] N. Chiabaut, M. Küng, M. Menendez, and L. Leclercq, "Perimeter control as an alternative to dedicated bus lanes: A case study," *Transp. Res. Rec., J. Transp. Res. Board*, vol. 2672, no. 20, pp. 110–120, Dec. 2018.

[55] I. I. Sirmatel and N. Geroliminis, "Stabilization of city-scale road traffic networks via macroscopic fundamental diagram-based model predictive perimeter control," *Control Eng. Pract.*, vol. 109, Apr. 2021, Art. no. 104750.

[56] S. F. A. Batista, D. Ingole, L. Leclercq, and M. Menéndez, "The role of trip lengths calibration in model-based perimeter control strategies," *IEEE Trans. Intell. Transp. Syst.*, vol. 23, no. 6, pp. 5176–5186, Jun. 2022.

[57] S. Gao, D. Li, N. Zheng, R. Hu, and Z. She, "Resilient perimeter control for hyper-congested two-region networks with MFD dynamics," *Transp. Res. B, Methodol.*, vol. 156, pp. 50–75, Feb. 2022.

[58] D. Sun, Z. Yin, and P. Cao, "An improved CAL3QHC model and the application in vehicle emission mitigation schemes for urban signalized intersections," *Building Environ.*, vol. 183, Oct. 2020, Art. no. 107213.

[59] D. Sun, K. Zhang, and S. Shen, "Analyzing spatiotemporal traffic line source emissions based on massive Didi online car-hailing service data," *Transp. Res. D, Transp. Environ.*, vol. 62, pp. 699–714, Jul. 2018.

[60] E. Barmpounakis, M. Montesinos-Ferrer, E. J. Gonzales, and N. Geroliminis, "Empirical investigation of the emission-macroscopic fundamental diagram," *Transp. Res. D, Transp. Environ.*, vol. 101, Dec. 2021, Art. no. 103090.

[61] S. F. A. Batista, G. Tilg, and M. Menéndez, "Exploring the potential of aggregated traffic models for estimating network-wide emissions," *Transp. Res. D, Transp. Environ.*, vol. 109, Aug. 2022, Art. no. 103354.

[62] M. Halakoo, H. Yang, and H. Abdulsattar, "Heterogeneity aware emission macroscopic fundamental diagram (e-MFD)," *Sustainability*, vol. 15, no. 2, p. 1653, Jan. 2023.

[63] C. Wan, X. Shan, P. Hao, and G. Wu, "Multi-objective coordinated control strategy for mixed traffic with partially connected and automated vehicles in urban corridors," *Phys. A, Stat. Mech. Appl.*, vol. 635, Feb. 2024, Art. no. 129485.

[64] A. Jamshidnejad, D. Sun, A. Ferrara, and B. De Schutter, "A novel bi-level temporally-distributed MPC approach: An application to green urban mobility," *Transp. Res. C, Emerg. Technol.*, vol. 156, Nov. 2023, Art. no. 104334.

[65] P. A. Lopez, M. Behrisch, L. Bieker-Walz, J. Erdmann, Y.-P. Flötteröd, R. Hilbrich, L. Lücken, J. Rummel, P. Wagner, and E. Wiessner, "Microscopic traffic simulation using SUMO," in *Proc. 21st Int. Conf. Intell. Transp. Syst. (ITSC)*, Maui, HI, USA, Nov. 2018, pp. 2575–2582. [Online]. Available: https://elib.dlr.de/124092/
[66] L. Codeca, R. Frank, and T. Engel, "Luxembourg SUMO traffic (LuST) scenario: 24 hours of mobility for vehicular networking research," in *Proc. IEEE Veh. Netw. Conf. (VNC)*, Dec. 2015, pp. 1–8.
[67] R. Saedi, R. Verma, A. Zockaie, M. Ghamami, and T. J. Gates, "Comparison of support vector and non-linear regression models for estimating large-scale vehicular emissions, incorporating network-wide fundamental diagram for heterogeneous vehicles," *Transp. Res. Rec., J. Transp. Res. Board*, vol. 2674, no. 5, pp. 70–84, May 2020.
[68] M. Wardman, P. W. Bonsall, and J. D. Shires, "Driver response to variable message signs: A stated preference investigation," *Transp. Res. C, Emerg. Technol.*, vol. 5, no. 6, pp. 389–405, Dec. 1997.
[69] T. Lomax, S. Turner, G. Shunk, H. Levinson, R. Pratt, P. Bay, and G. Douglas, "Quantifying congestion. Volume 2: User's guide," Transp. Res. Board, Washington, DC, USA, Tech. Rep., 1997.
[70] A. Wegener, M. Piórkowski, M. Raya, H. Hellbrück, S. Fischer, and J.-P. Hubaux, "TraCI: An interface for coupling road traffic and network simulators," in *Proc. 11th Commun. Netw. Simulation Symp.*, Apr. 2008, pp. 155–163.
[71] L. Ambühl, A. Loder, M. C. J. Bliemer, M. Menendez, and K. W. Axhausen, "A functional form with a physical meaning for the macroscopic fundamental diagram," *Transp. Res. B, Methodol.*, vol. 137, pp. 119–132, Jul. 2020.
[72] Y. Huang, D. Sun, A. Li, N. Garrick, S. Zhang, and W. Liu, "Spatiotemporal approach for evaluating the vehicle restriction policy with multi-sensor data," *Transp. Res. Rec., J. Transp. Res. Board*, vol. 2676, no. 8, pp. 724–736, Aug. 2022.
[73] E. W. Dijkstra, "A note on two problems in connexion with graphs," *Numerische Math.*, vol. 1, no. 1, pp. 269–271, Dec. 1959.
[74] K. Aboudolas, M. Papageorgiou, A. Kouvelas, and E. Kosmatopoulos, "A rolling-horizon quadratic-programming approach to the signal control problem in large-scale congested urban road networks," *Transp. Res. C, Emerg. Technol.*, vol. 18, no. 5, pp. 680–694, Oct. 2010.
[75] G. Perraki, C. Roncoli, I. Papamichail, and M. Papageorgiou, "Evaluation of an MPC strategy for motorway traffic comprising connected and automated vehicles," in *Proc. IEEE 20th Int. Conf. Intell. Transp. Syst. (ITSC)*, Oct. 2017, pp. 1–7.
[76] Z. Szalay, "Next generation X-in-the-loop validation methodology for automated vehicle systems," *IEEE Access*, vol. 9, pp. 35616–35632, 2021.

ALESSIO TESONE received the B.Sc. and M.Sc. degrees in automation engineering and the Ph.D. degree in transportation engineering from Universitã Degli Studi di Napoli Federico II, Naples, in 2017, 2020, and 2024, respectively. His research interest includes the modeling and control of urban traffic networks.

TAMÁS TETTAMANTI received the Ph.D. degree in traffic engineering from Budapest University of Technology and Economics, in 2013, and the D.Sc. degree in traffic engineering from the Hungarian Academy of Sciences, in 2023. He is currently an Associate Professor with the Faculty of Transportation Engineering and Vehicle Engineering, Budapest University of Technology and Economics. He participates in research and industrial projects both as a Researcher and a Project Coordinator. He is the coauthor of over 180 scientific articles, two patents, and several books. His current research interests include road traffic modeling, estimation and control in the cooperative, connected and automated mobility (CCAM) field, and related co-simulation technology developments. He is a member of the Public Body of the Hungarian Academy of Sciences. He is a member of the Technical Committee "TC 7.4 Transportation Systems" at the International Federation of Automatic Control (IFAC). He serves as an Editorial Board Member for IEEE TRANSACTIONS ON INTELLIGENT TRANSPORTATION SYSTEMS and *Communications in Transportation Research* journal (Elsevier).

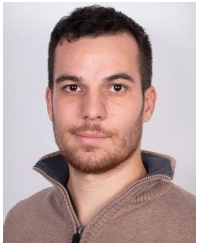

BALÁZS VARGA received the B.Sc. and M.Sc. degrees in vehicle engineering and the Ph.D. degree in traffic engineering from Budapest University of Technology and Economics, Budapest, Hungary, in 2013, 2015, and 2021, respectively. He was a Postdoctoral Researcher with the Chalmers University of Technology, Gothenburg, Sweden, in 2021. He is currently a Researcher with Budapest University of Technology and Economics. He has over 30 scientific publications. His research interests include the modeling and control of urban traffic networks with both classical and data-driven-based solutions.

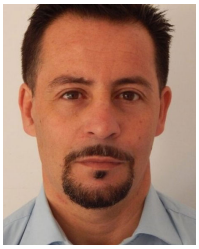

GENNARO NICOLA (CINO) BIFULCO received the M.Sc. degree in civil engineering from the University of Naples Federico II, Italy, in 1990, and the Ph.D. degree in transportation engineering from the University of Rome "La Sapienza," Italy, in 1993. He is currently a Full Professor with the University of Naples Federico II, where he is also the Director of the Studies for the Master's Degree in Transportation Engineering and Mobility. He is also the Coordinator of Spoke 7 (CCAM and Smart Infrastructures) of the Italian National Research Center for Sustainable Mobility. He is the author of one book on *Intelligent Transportation Systems*, several articles, and conference papers in the field of transportation and mobility. He holds one patent. His research interests include the modeling of driving, traveling, and mobility behaviors, intelligent transportation systems, advanced traveler information systems, advanced driving assistance systems, and cooperative connected and automated mobility. He is involved in the deploying process in Italy for developing smart roads and C-ITS solutions.

LUIGI PARIOTA received the M.Sc. and Ph.D. degrees in transportation engineering from the University of Naples Federico II, Naples, Italy, in 2009 and 2013, respectively. Since 2022, he has been an Associate Professor with the University of Naples Federico II, where he coordinates research activities on various topics, including the modeling of driving behavior, and the assessment of the impacts of new technologies on both drivers and traffic flow, urban traffic estimation and control, and mobility as a service.

Open Access funding provided by 'Università degli Studi di Napoli "Federico II"' within the CRUI CARE Agreement